Chapter 1 Introduction

Hyperfine-resolved optical transitions in molecular iodine (I_2) often provide stable references for precision spectroscopy [1, 2]. The narrow hyperfine components have also been widely used in laser frequency stabilization, following the lead of an early He-Ne/$^{127}I_2$ system by intracavity saturated absorption in a red laser at 633 nm [3]. Other systems include He-Ne/$^{127}I_2$ at 640, 612, 576, and 543 nm and Ar/$^{127}I_2$ at 515 nm as well as the $^{129}I_2$ variants. Most of these systems have wavelengths recommended for realization of the SI Metre [4].

The I_2 absorption lines near 532 nm are stronger than red transitions and are readily accessible by diode-pumped, frequency-doubled solid-state Nd:YAG lasers [5, 6]. The 532 nm system has generated a great deal of interests due to its inherently low frequency noise, compact size, high reliability, and relatively high powers and demonstrated high frequency stability ($< 5 \times 10^{-14}$ at 1 s) [7] better than the 633 nm iodine-stabilized He-Ne lasers. The 2001 meeting of Consultative Committee for Length (CCL) led the a_{10} component of R(56) 32-0 transition of $^{127}I_2$ at 532 nm for the optical frequency standard [8].

1.1 Motivation

The 532 nm system has been proved to be one of the best practical optical frequency standards and it will be the most important wavelength standard in the visible range in the future. The pressure shift and power shift of the a_{10} component have been reported [9]. However, the characteristics of the a_{10} component including linewidth, pressure broadening, and power broadening have not been investigated systematically. We hope to systematically investigate these characteristics as reference for those who study 532 nm systems for precision spectroscopy. We use the dependence of the peak amplitude of the third-derivative signal on the modulation width to determine the linewidth of the a_{10} component, and also

investigate its pressure and power broadening.

I_2 also provides a good subject with which to test theoretical models for Hamiltonian of hyperfine interactions [10]. For these interactions, the measured hyperfine splittings are fitted to a four-term Hamiltonian and the corresponding hyperfine constants could be obtained. In general, the hyperfine splitting is measured by heterodyne technique. Two lasers are independently stabilized to different hyperfine components and their frequency difference is obtained by measuring their beat frequency. However, not every laboratory could set up two iodine-stabilized lasers for measuring hyperfine splitting. For this reason, we try to use only one laser with a double-passed acousto-optic modulator (AOM) frequency shifter to measure the hyperfine splittings of R(56) 32-0 transition. We hope to offer an economically efficient method instead of replacing heterodyne technique to measure the hyperfine splittings especially as or while the laser is expensive.

Moreover, we are also interesting in using diode lasers for frequency stabilization. For diode lasers, their smaller size, larger tuning range, higher power, and compactness make them an attractive source for frequency stabilization. Frequency stabilization of the external cavity diode laser (ECDL) to the iodine hyperfine structure (HFS) components using extra-cavity iodine cell has been extensively studied and reported. In general, the frequency modulation is achieved by modulating the cavity length of the ECDL using a piezoelectric transducer. However, this modulation scheme limits the modulation frequency to <10 kHz. The frequency of ECDL can be also modulated by modulating current through the diode. The current modulation allows modulation frequency higher than PZT modulation for an ECDL. To reduce the noise, we choose to modulate the laser frequency by modulating the diode current instead of the cavity length by PZT.

We choose P(84) 5-5 transition of $^{127}I_2$ at 657.483 nm for our study. The reasons are as follows. First, the $^1S_0$-$^3P_1$ intercombination line of Ca at 657.459 nm has a linewidth much narrower than the HFS components of iodine. It is a useful reference for a precise optical

frequency standard. Recently we have developed a novel Ca absorption cell and successfully observed its saturation absorption spectrum with a linewidth below 300 kHz [11]. To further investigate the high resolution spectroscopy of the Ca, we want to develop a stable diode laser system at 657 nm as a stable light source. Second, the diode laser at 657 nm has the characteristics of lower cost and higher power than diode laser at 633 nm. It is an attractive alternative for red diode laser systems locked to iodine. Therefore, we investigate the saturation spectrum of the hyperfine components of P(84) 5-5 transition of $^{127}I_2$ at 657.483 nm for frequency stabilization of our ECDL.

1.2 Overview of This Dissertation

In Chapter 2, we introduce fundamental background knowledge in preparation for understanding the experiments and results in Chapter 3 ~ Chapter 5.

In Chapter 3, we determine the linewidth of the hyperfine structure a_{10} component of R(56) 32-0 transition of $^{127}I_2$ at 532 nm using the dependence of the peak amplitude of the third-derivative signal on the modulation width. We also use the same method to investigate pressure broadening and power broadening of the a_{10} component.

In Chapter 4, we describe that the hyperfine splitting of the iodine R(56) 32-0 transition at 532 nm is measured using a double-passed acousto-optic modulator frequency shifting apparatus. Preliminary results, compared with the values recommended by the Consultative Committee for Length, show that the accuracy is better than 20 kHz and it can be easily improved in the future.

In Chapter 5, the saturation spectrum of P(84) 5-5 transition of $^{127}I_2$ at 657.483 nm is also obtained with the third-harmonic demodulation method using an ECDL. The laser frequency is modulated by modulating the diode current instead of modulating the cavity length by PZT. Current modulation allows modulation frequency higher than PZT modulation. The

signal-to-noise ratio of 1000 is better than previous results in the literatures. The laser is frequency stabilized to the hyperfine component *o* of P(84) 5-5 transition with a frequency stability better than 10 kHz (2.2×10^{-11} relative stability).

In Chapter 6, we state the summary and future work.

References

[1] S. Ezekiel and R. Weiss, Phys. Rev. Lett. **20**, 91 (1968).

[2] M. D. Levenson and A. L. Schawlow, Phys. Rev. A **6**, 10 (1972).

[3] G. R. Hanes and C. E. Dahlstrom, Appl. Phys. Lett. **14**, 362 (1969).

[4] T. J. Quinn, Metrologia **30**, 523 (1994); and references therein.

[5] A. Arie, S. Schiller, E. K. Gustafson, and R. L. Byer, Opt. Lett. **17**, 1204 (1992).

[6] M. L. Eickhoff and J. L. Hall, IEEE Trans. Instrum. Meas. **44**, 155 (1995).

[7] J. Ye, L. Robertsson, S. Picard, L.-S. Ma, and J. L Hall, IEEE Trans. Instrum. Meas. **48**, 544 (1999).

[8] T. J. Quinn, Metrologia **40**, 103 (2003).

[9] K. Nyholm, M. Merimaa, T. Ahola, and A. Lassila, IEEE Trans. Instrum. Meas. **52**, 284 (2003).

[10] For example, L.-S. Chen, W. Y. Cheng and J. Ye, J. Opt. Soc. Am. B **21**, 820 (2004).

[11] M. S. Huang, M. H. Lu, and J. T. Shy, "A calcium vapor cell for atomic spectroscopy," Rev. Sci. Instrum. **73,** 3747 (2002).

Chapter 2 Background Knowledge

2.1 Molecular Iodine Spectrum

2.1.1 Ro-Vibrational Transitions of the B-X System

A large number of lines in the visible wavelength region were detected and originated from the $B^3\Pi_{u0}^+ - X^1\Sigma_g^+$ system in $^{127}I_2$ [1]. $B^3\Pi_{u0}^+$ is excited electronic state and $X^1\Sigma_g^+$ is ground electronic state for iodine molecule. Because of the extensive number of data and high resolution, the B-X system could be unambiguously analyzed [2] so precise rotational and vibrational molecular constants were calculated [3].

In a certain approximation, we may resolve the total energy of a molecule into the sum of vibrational, rotational, and vertical electronic energy. The vibrational energy is originated in the vibrational motions between atoms in molecules and the rotational energy is originated in the rotational motions about a certain axis. The vertical electronic energy comes from the electronic configuration between the electronic states of the molecule. Figure 2.1 shows the representation of the potential energy curves of the B and X states, where the electronic, vibrational, and rotational energy contributions are represented. The (') and (") indicate upper and lower state respectively. Most population is in $v''=0$ and $v''=1$ of the ground electronic state at room temperature due to the Boltzmann distribution.

For a rigid diatomic molecule the selection rule for rotational transition is ΔJ = J' - J" = ±1. The P branch is in which $\Delta J = -1$ and the R branch is in which $\Delta J = +1$. In our experiment, we use R(56) 32-0 transition of $^{127}I_2$ at 532 nm and P(84) 5-5 transition of $^{127}I_2$ at 657 nm as reference wavelengths. Figure 2.2 is the simple representation for these two transitions of $^{127}I_2$.

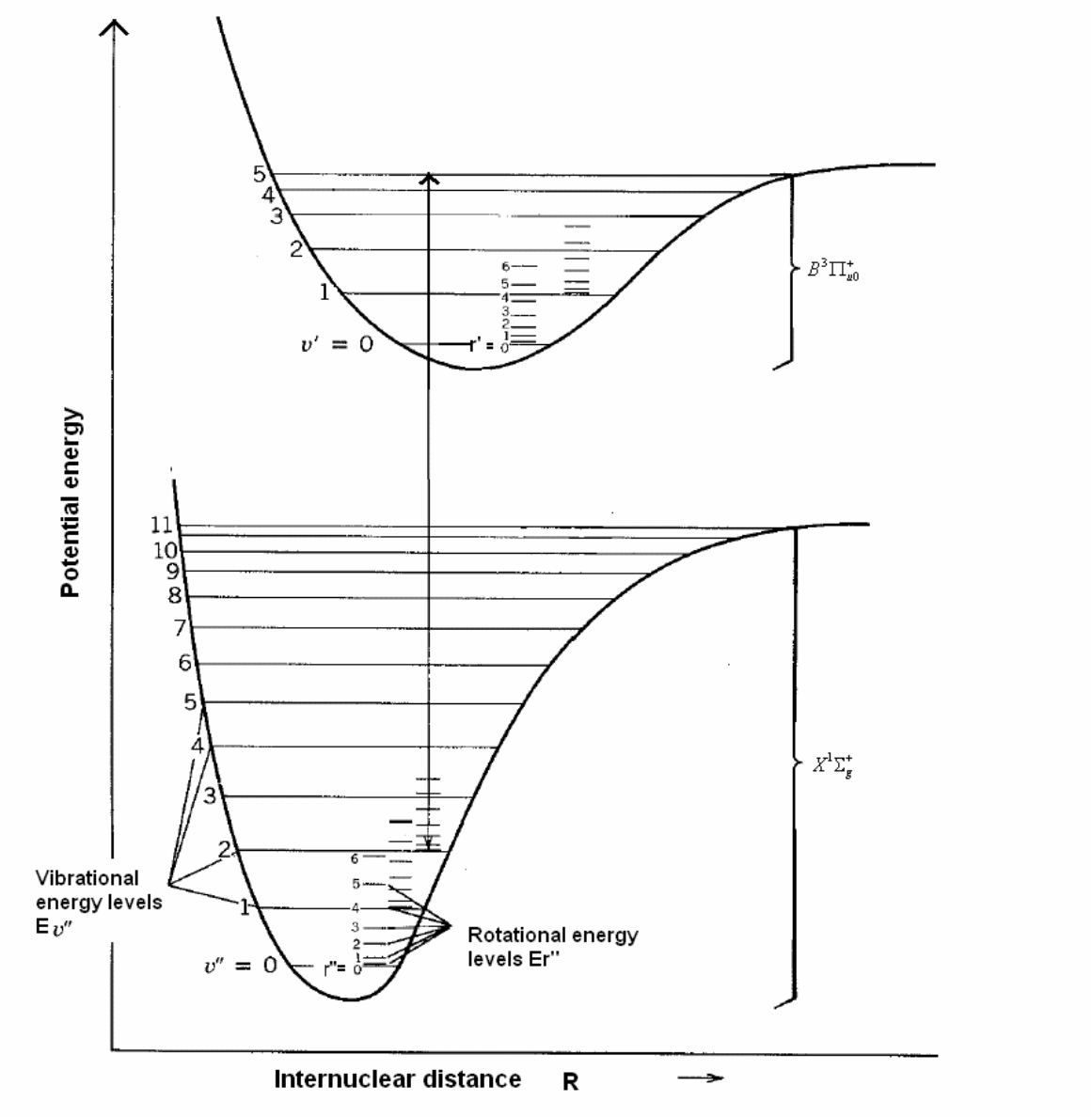

Fig. 2.1. Representation of the potential energy curves of the B and X states, where the electronic, vibrational, and rotational energy contributions are represented. The (’) and (”) indicate upper and lower state respectively.

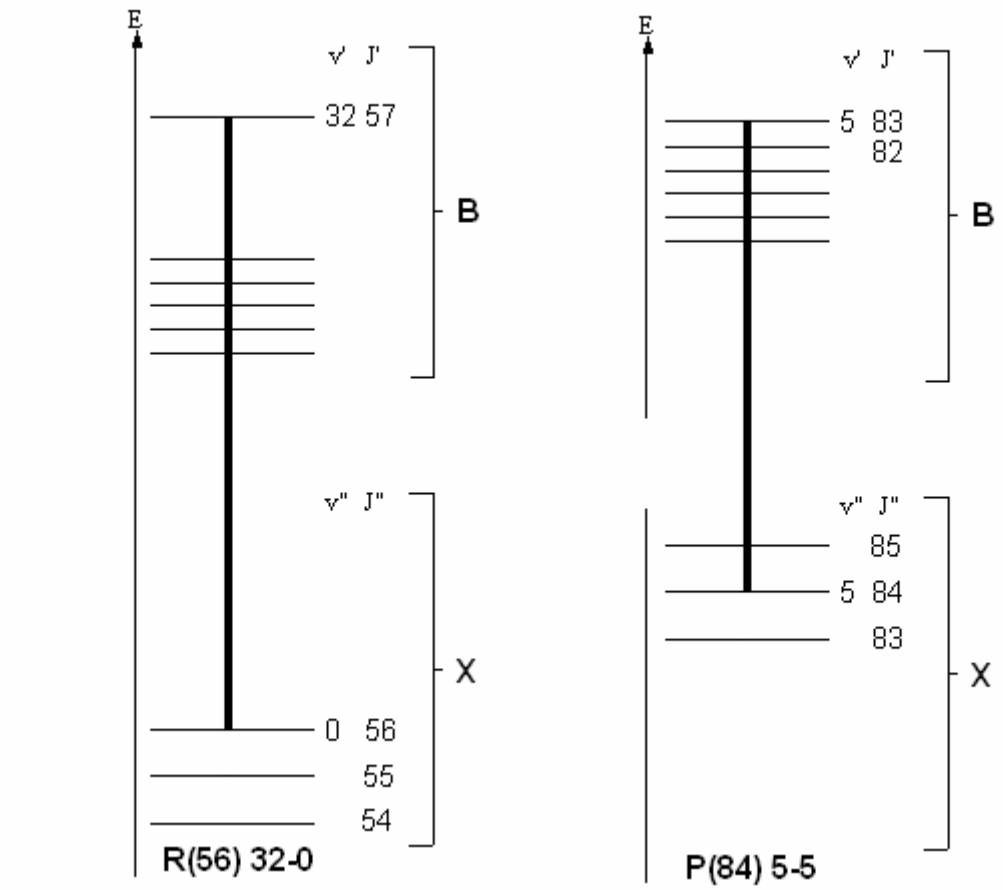

Fig. 2.2. Simple representation of ro-vibrational transitions of the B-X system of I_2 for R(56) 32-0 and P(84) 5-5.

2.1.2 Hyperfine structure

Moreover, the energy level could be splitted by the interaction between electrons and nucleus. The interaction between the electric or magnetic multipoles of nucleus of molecular iodine and the electromagnetic field arising from the other nucleus or electrons cause the hyperfine splitting in the rotational energy level [4]. In general, the Hamiltonian of the hyperfine structure of molecular I_2 can be expressed as:

$$H_{hfs} = eQq \times H_{EQ} + C \times H_{SR} + d \times H_{TSS} + \delta \times H_{SSS} \quad (1)$$

where H_{EQ}, H_{SR}, H_{TSS}, and H_{SSS} represent, respectively, the electric quadrupole, spin-rotation, tensor spin-spin, and scalar spin-spin interaction and eQq, C, d, and δ represent the corresponding hyperfine constant for each of these interactions. The other higher order term can also be included [5, 6], but we neglect them here. Since I_2 obeys Fermi-Dirac statistic. Its total wavefunction is anti-symmetric. For Born–Oppenheimer approximation, the total wave function can be expressed as:

$$\Psi = \Phi_e(R,r)\Phi_v\Phi_r\chi(1,2) \quad (2)$$

where Φ_e is the electronic total wave function. Φ_v is the vibrational part of nuclei and Φ_r is the rotational part of nuclei, and $\chi(1,2)$ is the spin function of nuclei. As exchanging of two nuclei,

$\Phi_e : X^1\Sigma_g^+$ is symmetric and $B^3\Pi_{u0}^+$ is antisymmetric.

Φ_v : It is always symmetric.

Φ_r : If J is even, it is symmetry. If J is odd, then it is anti-symmetric.

$\chi(1,2)$: Assume I=0, 2, 4, it is defined as para-state, an odd function. As I=1, 3, 5, it is defined as ortho-state, an even function.

Where v is the vibrational quantum number. J is the rotational quantum number and I is the nuclear spin. For an energy level J, it has splitting sub energy levels which are labeled by

F and I ($\vec{F} = \vec{I} + \vec{J}$). In order to preserve the total wave function as anti-symmetry at exchanging two nuclei, not all the sub-level energy exist. Hence, for $X^1\Sigma_g^+$ state, it exists 15 sub-energy levels in even J and 21 sub-energy levels in odd J. For $B^3\Pi_{u0}^+$ state, there are 15 sub levels, as J is odd; there are 21 sub levels as J is even. For R(56) 32-0 transition and P(84) 5-5 transition, they have 15 sub-energy levels, respectively. The transitions between the sub levels in different electronic state obeying the selection rule $\Delta I = 0$ and $\Delta F = \Delta J = \pm 1$ (J>> I) lead to the strongest hyperfine structures in the spectroscopy. These transitions are called "main lines". These transitions of the hyperfine structure components in a ro-vibrational transition are sometimes named a, b, c, d….in decreasing frequency order. It has also been suggested that the components could be named in increasing frequency order [7], a_1, a_2, a_3….

2.2 Widths of Spectral Lines

The Lorentzian line profile with the natural linewidth cannot be observed without special techniques, because it is completely concealed by other broadening effects. One of the major contributions to the spectral linewidth in gases at low pressures is the Doppler width, which is due to the thermal motion of the absorbing or emitting molecules. In gases of diatomic and polyatomic molecules, the molecular collision induces transitions between rotational levels and less frequently between vibrational levels. Since the collision frequency is proportional to the gas pressure, the collision-induced additional line broadening is therefore often called pressure broadening. Moreover, at sufficiently large laser intensities, the optical pumping rate on an absorbing transition becomes larger than the relaxation rates. The linewidth increases with the optical field intensity. This broadening effect is called power broadening.

2.3 Saturation Spectroscopy

The study of saturation spectroscopy began just after the first gas laser invented by Javan et al. [8]. Until 1969, the first frequency stabilization laser was realized by Barger and Hall by using the saturation spectroscopy method [9]. They stabilized 3.39 μm HeNe laser to CH_4 transition. In 1973, Hanes and Dahlstrom locked 633 nm HeNe laser to $^{127}I_2$ transition [10]. Thereafter the method of saturation spectroscopy is widely applied in frequency stabilization of lasers. It is one of the most efficient and promising methods in regard to both fundamental and applied works.

Saturation spectroscopy is based on the velocity-selective saturation of Doppler-broadened transition because molecules or atoms obey Maxwell-Boltzmann velocity distribution. Its fundamental scheme is two laser beams propagating in the absorption medium with opposite directions. An experimental realization of saturation spectroscopy is illustrated in Fig. 2.3. A pump beam passes through a gaseous sample of molecules with a

Maxwell-Boltzmann velocity distribution. The reflected beam from a mirror which is fraction of the pump beam is the probe beam. The probe beam is detected by a photodiode after passing through a quarter wave plate (λ/4) and a polarizing beam splitter (PBS).

Fig. 2.4 (a) shows the pump beam and probe beam interact with different groups of molecules or atoms with the same speed but opposite direction as the laser frequency off the resonance. Therefore, the two laser beams burn two holes in the population curve. Fig. 2.4 (b) shows both beams are absorbed by the same molecules with axial velocity equal to zero while the laser frequency is resonant with the absorption of the medium. The Doppler-broadened absorption profile with a Lamb dip [11] is shown.

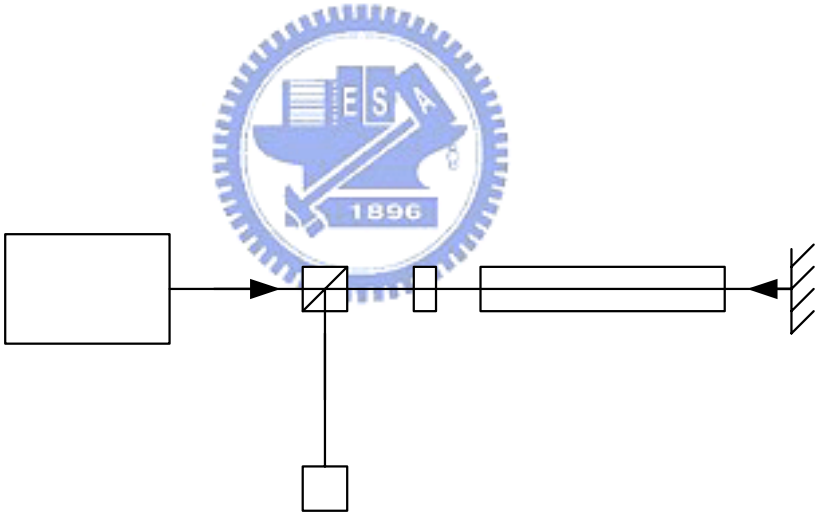

Fig. 2.3. Experimental setup for saturation spectroscopy. PBS, polarization beam splitter; λ/4, quarter wave plate.

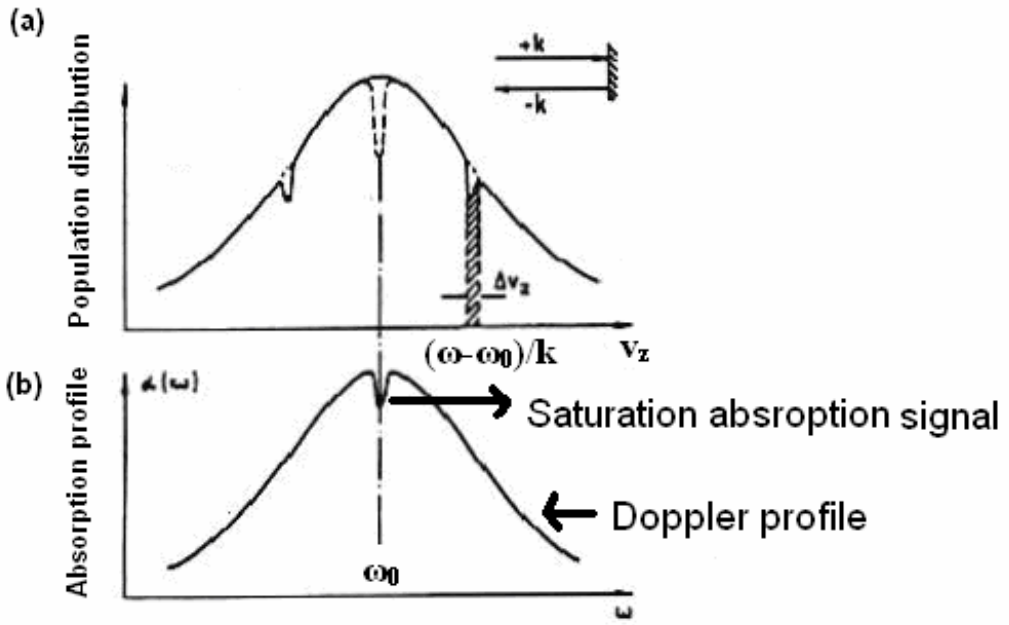

Fig. 2.4 a-b. Saturation of an inhomogeneous line profile: (a) Bennet holes caused by the two counterpropagating laser beams for $\omega \neq \omega_0$ and for $\omega = \omega_0$ (dashed curve) (b) Lamb dip in the absorption profile [12].

2.4 Third-Harmonic Demodulation Method

The saturation absorption signal is usually very small and it is easily obscured by noise sources. Therefore, to reduce noise around signal and to rise signal-to-noise ratio (SNR) are needed. The most used method is to modulate laser frequency and to demodulate saturation absorption signal by using a lock-in amplifier where we can obtain the harmonic signals of the saturation spectrum. In general, the methods to modulate laser frequency include vibrating a piezoelectric transducer (PZT) of a laser cavity to change the length of the laser cavity, modulating driving current of diode laser or making a laser beam pass through an electro-optic modulator (EOM).

Lock-in amplifiers are used to detect and measure very small AC signals. They use a technique known as phase-sensitive detection (PSD) to single out the component of the signal at a specific reference frequency and phase. Noise signals at frequencies other than the reference frequency are rejected by the low pass filter and do not affect the measurement. Only inputs frequencies at the reference frequency result in an output. In general, the PSD is done by using a lock-in amplifier, where the rf-modulated signal output of the detector is mixed with the *n*th ($n\omega$) frequency component as a reference signal. After the output from the mixer passes through a bandpass filter, we can finally obtain the *n*th harmonic. In other words, the PSD means to find the *n*th component (harmonic) of the Fourier series of the rf-modulated signal.

The saturation absorption signal can be described as Lorentzian profile

$$L(\nu-\nu_0)=\frac{1}{1+[\frac{2(\nu-\nu_0)}{\delta L}]^2} \tag{3}$$

where ν is laser frequency, ν_0 is resonance frequency, and δL is full width at half maximum (FWHM) of saturation absorption signal. Frequency modulation can be described by

$$\nu(t)=\nu+W\cos\omega t \tag{4}$$

where W is modulation amplitude and ω is modulation angular frequency.

From Eqs. (1) and (2), the Lorentzian profile is rewritten as

$$I(\alpha,\beta)=\frac{1}{1+(\alpha+\beta\cos\omega t)^2} \tag{5}$$

where $\alpha=\frac{2(\nu-\nu_0)}{\delta L}$ and $\beta=\frac{2W}{\delta L}$. Since *I(α,β)* is a periodic and even function of ωt, it can be expressed as a Fourier series

$$I(\alpha,\beta)=\frac{a_0}{2}+\sum_{n=1}^{\infty}H_n(\alpha,\beta)\cos n\omega t \tag{6}$$

where $H_n(\alpha,\beta)$ is the *n*th Fourier coefficient. When the saturation absorption signal is demodulated by $n\omega$, the Lorentzian profile would be transformed into H_n. Because the *n*th-derivative profile of the Lorentzian profile is similar to the *n*th-Fourier coefficient $H_n(\alpha, \beta)$, we use computer to simulate the *n*th-derivative profile of the Lorentzian profile and help us understand the *n*th-Fourier coefficient $H_n(\alpha, \beta)$. Figure 2.5 shows a Lorentzian profile and its *n*th derivative profiles with n=1, 2, 3. Nakazawa has analyzed the property of H_n in 1986 [13].

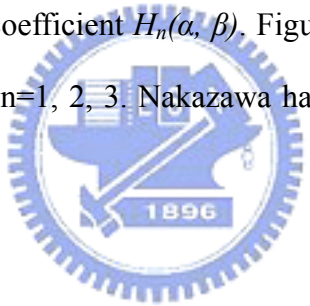

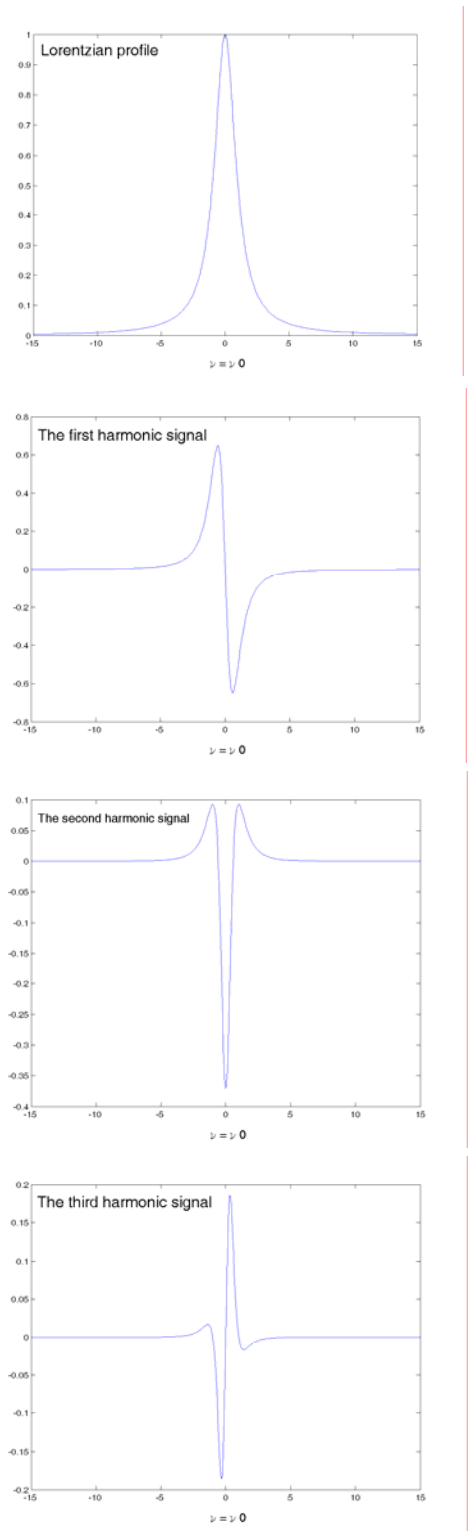

Fig. 2.5. Lorentzian profile and its harmonic demodulation profiles of H_n with n=1, 2, 3 by using computer simulation.

The harmonic demodulation signals of the saturation spectrum can be used for frequency stabilization of a laser. However, they must satisfy following requirements:

A. No background: Background will produce frequency shift. If there is a background existing in a harmonic signal we must offer an offset voltage to compensate the background. Even though we lock the laser at the zero point of the harmonic signal, the compensation is needed.

B. Odd function: Only the odd harmonic function offers enough information to tell us whether the laser frequency is ahead or behind the center frequency.

C. High SNR: The stability of the frequency stabilization is dependent on SNR of signal.

The SNR of the first harmonic signal is larger than that of the third harmonic signal; however the Doppler background evidently exists in the first harmonic signal. Moreover, the Doppler background is almost removed under the third harmonic signal. The fifth harmonic signal shows too small SNR. Therefore, we choose the third harmonic signal to be employed in our experiments.

Nakazawa analyzed the relationship between slope sensitivity of nth derivatives and normalized modulation width [13]. The relationship is shown in Fig. 2.6. It is very useful for obtaining the optimum frequency stabilization condition at the line center of Lorentzian shape. The maximum slope of -0.77 for the first derivative is attained at normalized modulation width of 0.71. For the third derivative signal, the slope is 0.34 at normalized modulation width of 1.64. That means the third harmonic signal has the maximum slope and enables the laser spectrometer system to obtain optimal frequency stability when modulation width is 1.64 times the FWHM of the saturation absorption signal. The slope becomes -0.21 at normalized modulation width of 2.63 for the fifth derivative signal.

Due to the profile of the third harmonic signal is similar to the third derivative profile of the Lorentzian profile; the name of the third derivative signal is also employed.

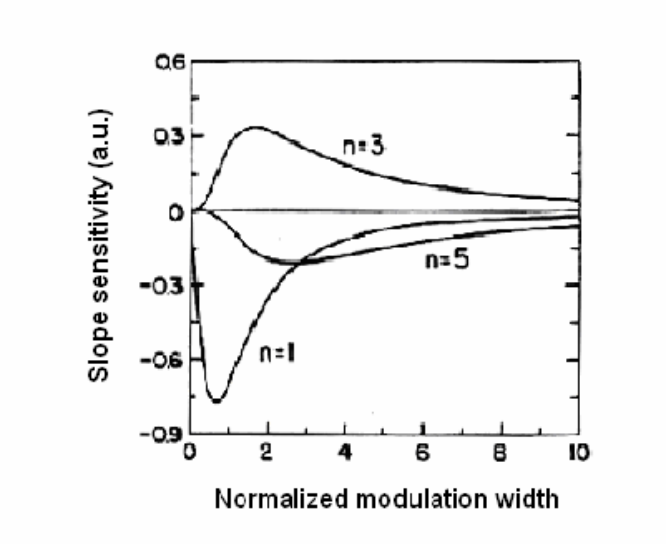

Fig. 2.6. Relationship between slope sensitivity of nth derivatives and normalized modulation width [13].

2.5 Linewidth Determination (Using the dependence of the peak amplitude of the third-derivative signal on the modulation width)

Line profiles are often investigated by means of a modulation process. By this process the static profile is converted into a periodically alternating signal allowing the well-established techniques of PSD to be applied. PSD produces a derivative of the line profile, that is, one of the harmonics that appear at the rf output, by sweeping the field frequency with a certain amount of frequency modulation. Consequently the demodulated signal depends on the form of the line profile and also on the amplitude and the spectral purity of the modulation. The demodulated signals have been derived on the assumption of a pure harmonic modulation [13,14]. We will briefly review the derivation following the work by Bayer-Helms and Helmcke [14].

The line profile may be mathematically described by a function f(d), in which d is the modulated quantity measured in intervals of the frequency. At first an exactly harmonic modulation

$$d = d_M + d_A \cos\omega t \qquad (7)$$

may be assumed at the instantaneous mean value $d = d_M$ with the modulation amplitude d_A (> 0) and the modulation angular frequency ω. The periodic signal can be expressed by a Fourier series:

$$f(d_M + d_A \cos\omega t) = A_0/2 + \sum_{m=1}^{\infty} (A_m \cos m\omega t + B_m \sin m\omega t) \qquad (8)$$

The corresponding Fourier coefficients or signal coefficients A_m and B_m give the amplitudes of the higher harmonics in the signal as well as their phase relations to the modulation (7). They are calculable according to equation

$$A_m + iB_m = 1/\pi \int_0^{2\pi} f(d_M + d_A \cos\omega\tau)\, e^{im\omega\tau}\, d\tau, \qquad m \geqq 0 \qquad (9)$$

if the profile function f(d) is known. By bisection of the interval 2π of the integrals in (9) one

obtains

$$A_m = 2/\pi \int_o^{\pi} f(d_M + d_A \cos\omega\tau) \cos(m\omega\tau) d\tau, \qquad B_m = 0 \qquad (10)$$

which means that if the modulation is described by cosωt, the phase relations of all harmonics are always given by cos mωt.

For Lorentzian profile,

$$f(d) = 1/(1+\delta^2) \qquad (11)$$

The symbol δ designates the dimensionless quantity of d divided by the half width at half maximum d_H:

$$\delta = d/d_H \qquad \delta_M = d_M/d_H \qquad \delta_A = d_A/d_H \qquad (12)$$

The Fourier coefficient A_m gives the amplitude of the higher derivative signal of the Lorenzian line profile. The first four Fourier coefficients for the Lorentzian profile are [14]

$$P_{\pm} = (2(\rho \pm \alpha))^{0.5}/\rho \qquad \rho = (\alpha^2 + 4\delta_M^2)^{0.5} \qquad \alpha = 1 + \delta_A^2 - \delta_M^2 \qquad (13)$$

$$A_0 = P_+ \qquad (14)$$

$$A_1 = ((\mathrm{sgn}\delta_M)P_- - \delta_M P_+)/\delta_A \qquad (15)$$

$$A_2 = (-4|\delta_M|P_- - (2(1-\delta_M^2)+\delta_A^2)P_+ + 4)/\delta_A^2 \qquad (16)$$

$$A_3 = ((-\mathrm{sgn}\delta_M)(4(1-3\delta_M^2) + 3\delta_A^2)P_- + (4(3-\delta_M^2) + 3\delta_A^2)\delta_M P_+ - 16\delta_M)/\delta_A^3 \qquad (17)$$

The analytical form of the peak amplitude of the first-derivative signal on the normalized modulation width δ_A has been derived by M. Nakazawa [13]. The formula is as follows:

$$f(\delta_A) = \frac{\sqrt{3}[(4+3\delta_A^2)^{1/2} - 2]}{2\delta_A[(4+3\delta_A^2)^{1/2} - 1]^{1/2}}. \qquad (18)$$

For the second- and third-derivative signals, no analytical formula has been derived for the peak amplitude on the modulation width. We can obtain the second-derivative signal as a function of δ_M for different δ_A using Eq. (16), we then determine the peak amplitude from the

second-derivative signal. We try to find out an analytical formula for the peak amplitude vs. the normalized modulation width. We use software of "Origin" to carry out this thought. After many times tries, we have the best result. We propose following analytical formula for the peak amplitude vs. the normalized modulation width:

$$g(\delta_A) = (P_1\delta_A + P_2\delta_A^2)/(P_3 + P_4\delta_A + P_5\delta_A^2 + P_6\delta_A^3). \quad (19)$$

The fitted coefficients are: $P_1 = -0.06795$, $P_2 = 1.20627$, $P_3 = 7.688$, $P_4 = 2.63378$, $P_5 = 3.11903$, $P_6 = 0.13152$. The uncertainty is 10^{-7}. Figure 2.7(a) shows the peak amplitude of the second-derivative signal as a function of the normalized modulation width (dotted points) and the curve of the analytical function $g(\delta_A)$ (solid line).

The peak amplitude of the third-derivative signal on the normalized modulation width is also analyzed similarly by the software of "Origin". The fitted function is

$$h(\delta_A) = (P_1\delta_A + P_2\delta_A^2 + P_3\delta_A^3)/(P_4 + P_5\delta_A + P_6\delta_A^2 + P_7\delta_A^3). \quad (20)$$

The fitted coefficients are: $P_1 = -1.51636$, $P_2 = 6.89591$, $P_3 = -0.09229$, $P_4 = 48.96763$, $P_5 = -3.70996$, $P_6 = 16.56378$, and $P_7 = 1.93711$. The uncertainty is 10^{-7}. Figure 2.7(b) shows the peak amplitude of the third-derivative signal as a function of the normalized modulation width (dotted points) and the curve of the analytical function $h(\delta_A)$ (solid line). The difference between the peak amplitude and the analytical function curve is less than 1 % for both analytical functions $g(\delta_A)$ and $h(\delta_A)$.

(a)

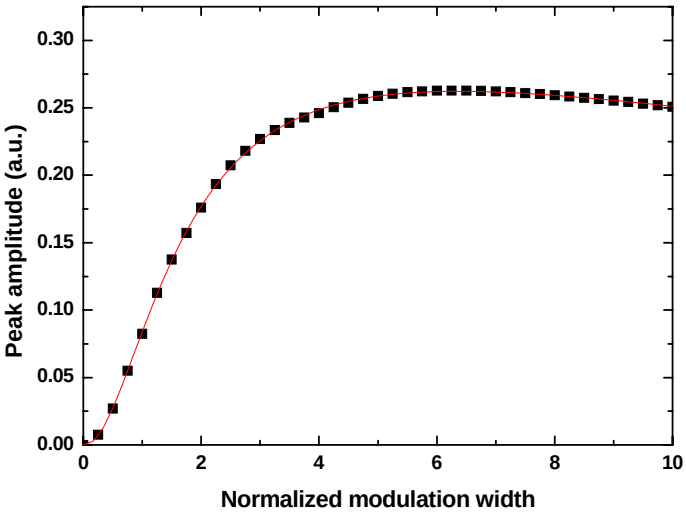

(b)

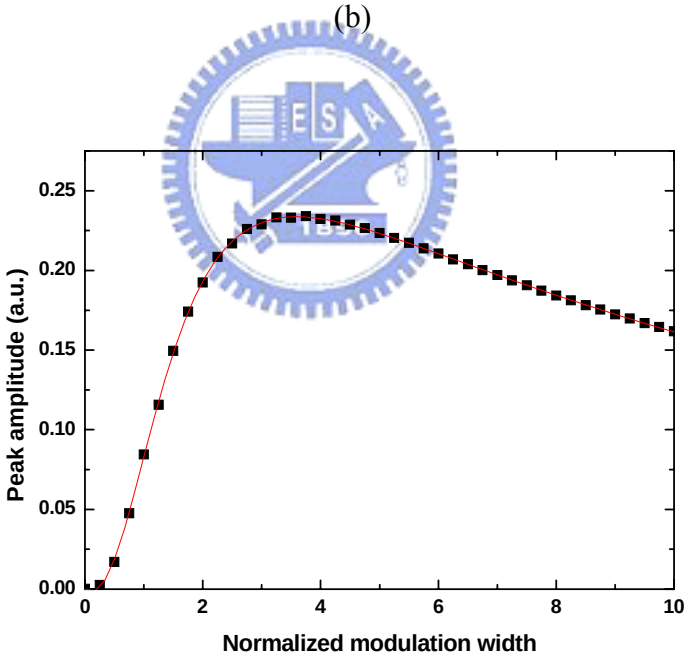

Fig. 2.7. (a) The peak amplitude of the second-derivative signal vs. the normalized modulation width (dotted points) and the curve of the analytical function $g(\delta_A)$ (solid line). (b) The peak amplitude of the third-derivative signal vs. the normalized modulation width (dotted points) and the curve of the analytical function $h(\delta_A)$ (solid line).

References

[1] S. Gerstenkorn and P. Luc, Atlas du spectre d'absorption de la molecule d'iode 14800-20000 cm-1, (CNRS 1978).

[2] S. Gerstenkorn and P. Luc, Atlas du spectre d'absorption de la molecule d'iode 14800-20000 cm-1. Complement: Identification des transitions du systeme (B-X), (CNRS 1985).

[3] S. Gerstenkorn and P. Luc, J. Physique **46**, 867 (1985).

[4] Arimondo, E., N. Inguscio and P. Violino, Rev. Mod. Phys. **49**, 31 (1977).

[5] A. Yokozeki and J.S. Muenter, J. Che. Phys. **72**, 3796 (1980).

[6] L.A. Hackle, *et al*., Phys. Rev. Lett. **35**, 568 (1975).

[7] M. Gläser, CCDM/82-32.

[8] A. Javan, W. R. Bennet, JR., and D. R. Herriott, Phys. Rev. Lett. **6**, 106 (1961).

[9] R. L. Barger and J. L. Hall, Phys. Rev. Lett. **22**, 408 (1969).

[10] G. R. Hanes and C. E. Dahlstrom, APPL. Phys. Lett. **14**, 362 (1973).

[11] W. E. Lamb, Phys. Rev. A **134**, 1429 (1964).

[12] W. Demtröder, Laser Spectroscopy, The third edition, Springer-Verlag Heidelberg New York, 451 (2003).

[13] M. Nakazawa, J. Appl. Phys. **59** 2297 (1986).

[14] F. Bayer-Helms and J. Helmcke, PTB-Bericht. **Me-17**, 85 (1977).

Chapter 3

Study Saturation Spectroscopy of R(56) 32-0 Transition of Molecular Iodine at 532 nm

3.1 Background Introduction

3.1.1 Literature Review

Optical frequency standards are of great interests not only for metrology applications but also for high-resolution spectroscopy, optical communications and fundamental physics. In recent years, diode-pumped solid state laser systems have been targeted as the ideal sources for optical frequency standards. The diode-pumped, frequency doubled Nd:YAG laser at 532 nm has generated a great deal of interests due to its inherently low frequency noise, small size, high reliability, and relatively high powers. Since the observation of hyperfine components of iodine transitions near 532 nm and the laser frequency stabilization based on the observed transitions using FM side-band spectroscopy [1,2], iodine-stabilized Nd:YAG lasers have demonstrated stabilities better than the 633 nm iodine-stabilized He-Ne lasers [3]. The 2001 meeting of Consultative Committee for Length (CCL) led the a_{10} component of R(56) 32-0 transition of $^{127}I_2$ at 532 nm for the optical frequency standard [4]. It will be the most important wavelength standard in the visible range in the future. Its pressure shift and power shift has been reported [5]. However, the characteristics of the a_{10} component including linewidth, pressure broadening, and power broadening have not been investigated systematically yet.

3.1.2 Research Outline

In this chapter we use the dependence of the peak amplitude of the third-derivative signal on the modulation width (PAM from now on, described in Chapter 2) to determine the

linewidth of the a_{10} component, and also investigate its pressure and power broadened. To verify the accuracy of this linewidth determination method, we measure the FWHM linewidth of the a_{10} component using the conventional saturation spectroscopy method. The experimental line profile obtained using the saturation spectroscopy method will be fitted with Lorentzian profile to compare the accuracy of measurement.

3.2 Experimental Setup

The experimental setup is shown in Fig. 3.1. We use a 450 mW monolithic diode-pumped non-planar ring oscillator (NPRO) Nd:YAG laser (Lightwave Electronics Model 126) as the light source. The NPRO laser has the good characteristics of narrow linewidth (less than 5 kHz), low frequency drifts (less than 50 MHz/h), and wide single mode tuning range (larger than 35 GHz). Its frequency can be tuned by changing the temperature of the laser crystal (thermal tuning), or applying a voltage on the PZT attached on the laser crystal. The former has a slow response time of few seconds and the latter has a response bandwidth of 100 kHz.

The laser beam passes through a 30 dB Faraday isolator to reduce the optical feedback effect and then passes through a half wave plate (λ/2) into a periodically poled $LiNbO_3$ (PPLN) crystal. The PPLN crystal is 50-mm long and 0.5-mm thick with a 6.5 μm period. The PPLN is heated to 53 ^{o}C for quasi-phase-matched frequency doubling. The λ/2 is used to adjust the light polarization to match the PPLN z-direction. The output wavelengths from the PPLN crystal include fundamental 1064 nm and second harmonic 532 nm. They are separated by a harmonic separator. This harmonic separator is a dichroic beam splitter which separates the Nd:YAG fundamental from its second harmonic. The 1064 nm beam is transmitting and the other 532 nm beam is reflected. Then the 532 nm beam passes through an IR filter to further filter out the residual 1064 nm radiation. The 532 nm laser output then enters a 10-cm long iodine cell as the pump beam. A neutral density (ND) filter is used to adjust the power of the pump beam. A fraction of the pump beam reflected from a 40 % partial reflection mirror (PRM) is the probe beam. The probe beam is detected by a photodiode after passing through a quarter wave plate (λ/4) and a polarizing beam splitter (PBS).

The Doppler-free saturation spectrum of hyperfine components of R(56) 32-0 transition is observed using the conventional third-harmonic demodulation method with a lock-in amplifier and is recorded by a chart recorder. The lock-in amplifier we use is SR830 from

Stanford Research Systems which has the ability to demodulate the signal at any harmonic up to 19999. In our experiment, we use the sine out of the lock-in amplifier at 10 kHz to modulate the Nd:YAG laser frequency and choose the third-harmonic of 10 kHz (i.e. 30 kHz) to demodulate a_{10} signal. The time constant of the lock-in amplifier is 300 μs. The laser frequency is scanned by applying a triangular signal to the PZT.

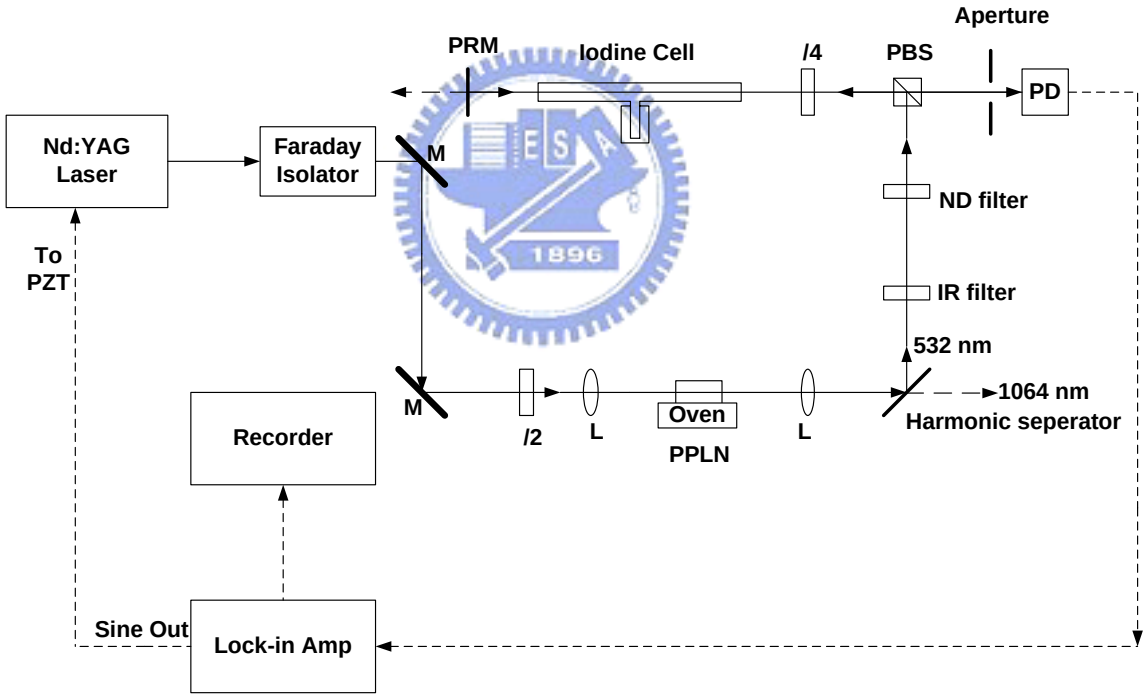

Fig. 3.1. Experimental setup. M, mirror; λ/2, half wave plate; L, lens; PPLN, periodically poled $LiNbO_3$; ND filter, neutral density filter; PBS, polarizing beam splitter; λ/4, quarter wave plate; PRM, partial reflection mirror; PD, photodiode.

3.3 Results and Discussion

3.3.1 PAM Method

Figure 3.2 is the whole hyperfine components of R(56) 32-0 transition. We first use the a_{10} component to check the PAM method. The third-derivative signal of a_{10} is obtained using the third-harmonic demodulation method. The pump beam power is 4.75 mW and the vapor pressure of the iodine cell is kept at about 4.1 Pa. The pump beam size in the center of the iodine cell is about 1.3 mm in diameter. When the Nd:YAG laser is modulated by the sine output from the lock-in amplifier, we record the third-derivative signal of hyperfine component a_{10}. We then measure the peak amplitude of the third-derivative signal.

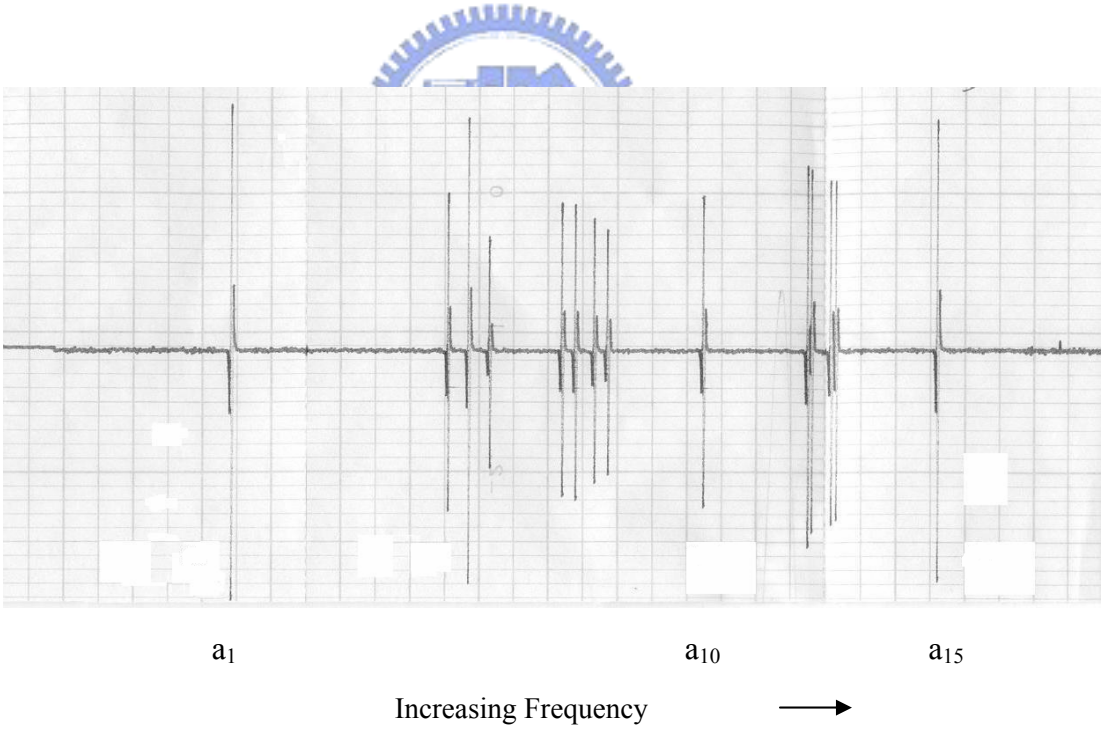

Fig. 3.2. The whole hyperfine components of R(56) 32-0 transition of $^{127}I_2$ at 532 nm.

We determine the linewidth by fitting the experimental points to equation $h(\delta_A)$ (Eq. 20). Figure 3.3 shows the peak amplitude of the third-derivative signal vs. the modulation width. The dotted points are the experimental data. The solid line in Fig. 3.3 is the fitted curve. The experimental data agree with the fitted curve very well. The FWHM width of the a_{10} component determined by PAM is 1.755 MHz with a standard deviation of 0.044 MHz.

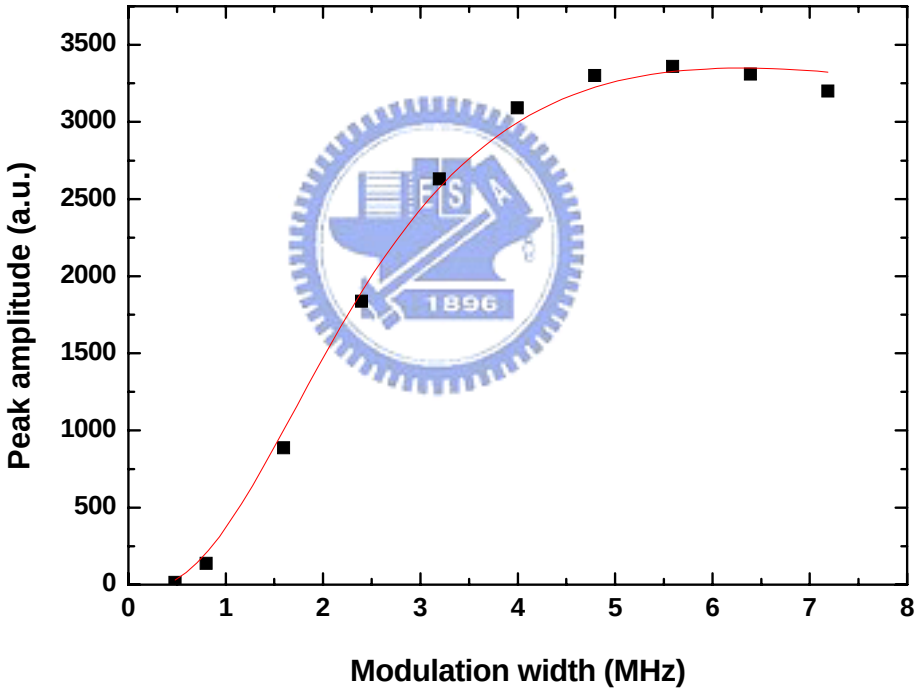

Fig. 3.3. The measured peak amplitude of the third-derivative signal vs. modulation width (dotted points) and the fitted curve (solid line). The fitted FWHM width of the a_{10} component is 1.755±0.044 MHz.

To verify the PAM measurement, we measure the a_{10} linewidth using the saturation spectroscopy method. The experimental setup is shown in Fig. 3.4. The second-harmonic 532 nm beam after PPLN is divided into two beams with 1.5 and 6.5 mW respectively. We lock the Nd:YAG laser to the a_6 component of R(56) 32-0 transition using the 1.5 mW beam. The experimental setup shown in Fig. 3.1 is used to obtain the third-derivative signal for stabilizing the laser frequency. The 6.5 mW beam enters a double-passed acousto-optic modulator (AOM) frequency shifter to generate a frequency tunable beam (The detailed working principle of the double-passed frequency shifter has been described in **4.2** of Chapter 4). This frequency shifted beam is used to scan the saturation spectroscopy of the a_{10} component of R(56) 32-0 transition.

We should measure the a_{10} linewidth directly. However, the Nd:YAG laser is frequency modulated in the experiment and the linewidth of the 532 nm laser beam becomes 2 MHz, not the original linewidth of 5 kHz. First we must eliminate or reduce the broadened linewidth due to the modulation process. Our method is to use the AOM frequency shifter to reduce the modulation process on the Nd:YAG laser. Figure 3.5 is the experimental setup.

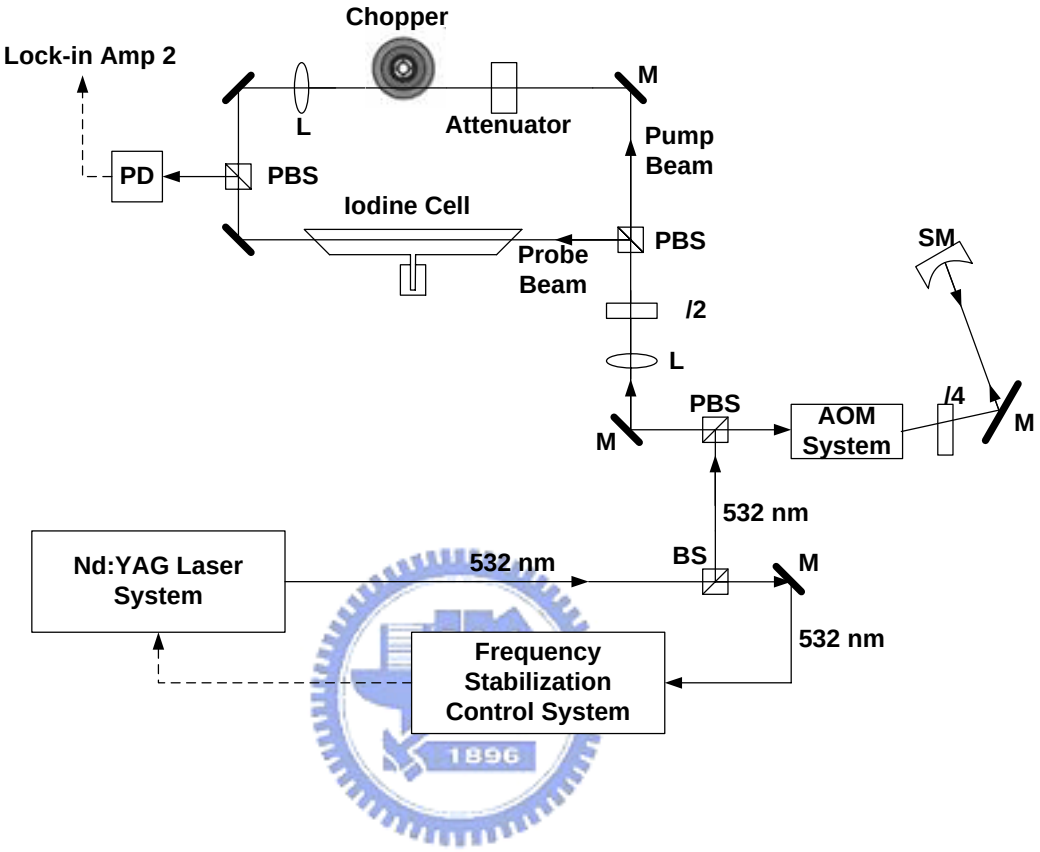

Fig. 3.4. Experimental setup for saturation spectroscopy of the a_{10} component of R(56) 32-0 transition. BS, beam splitter; M, mirror; λ/2, half wave plate; L, lens; PBS, polarizing beam splitter; PD, photodiode; AOM, acousto-optic modulator; SM, spherical mirror (concave).

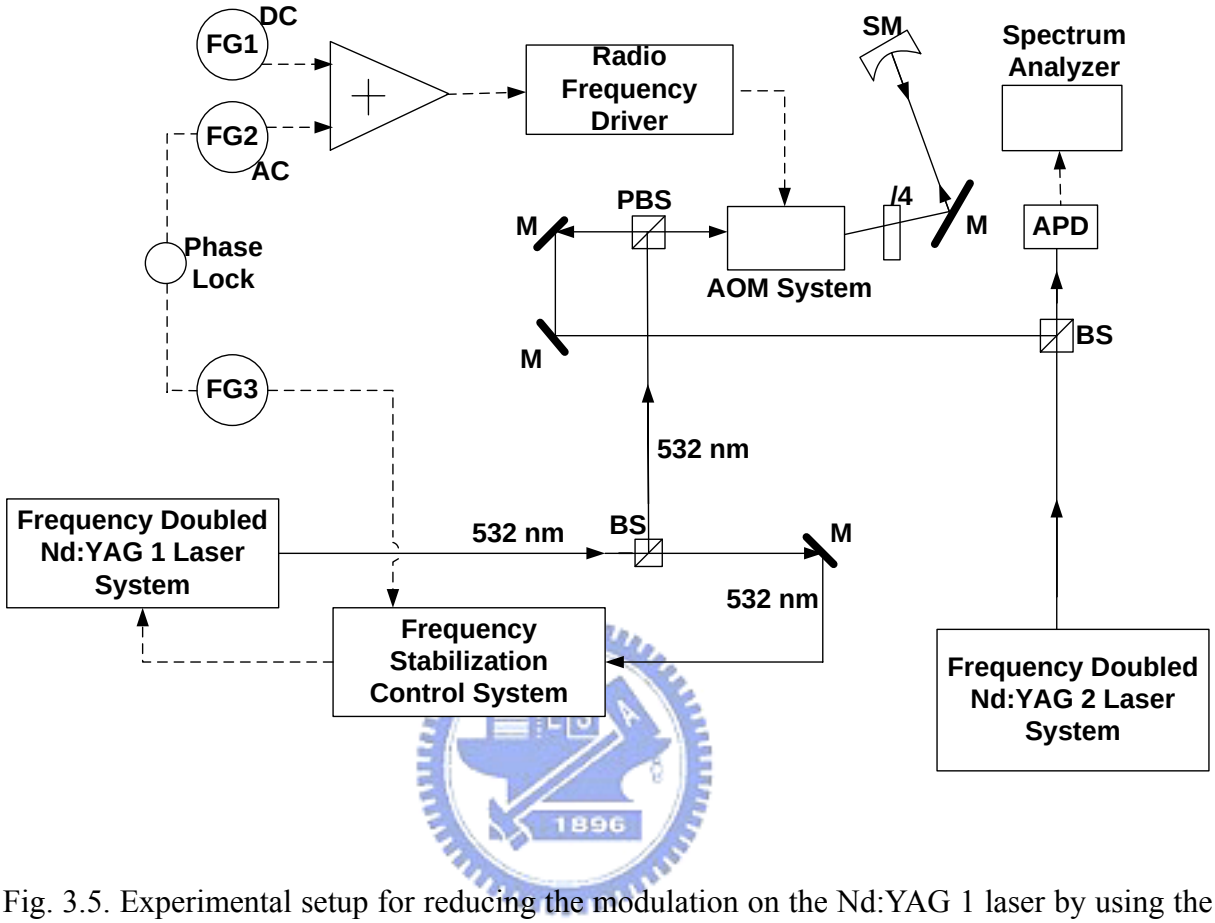

Fig. 3.5. Experimental setup for reducing the modulation on the Nd:YAG 1 laser by using the AOM frequency shifter. BS, beam splitter; M, mirror; PBS, polarizing beam splitter; APD, avalanche photodiode; AOM, acousto-optic modulator; SM, spherical mirror (concave); FG, function generator.

In Figure 3.5, the second-harmonic 532 nm beam of the Nd:YAG 1 laser is divided into two beams with 1.5 and 6.5 mW respectively. We lock the Nd:YAG 1 laser to the a_6 component of R(56) 32-0 transition using the 1.5 mW beam. The 6.5 mW beam enters the double-passed AOM frequency shifter and the first-order diffracted beam is selected. Then the first-order diffracted beam is sent into an avalanche photodiode (APD) with another 532 nm laser beam which is from the Nd:YAG 2 laser system. There are no modulation process on the Nd:YAG 2 laser. Finally, the two signals are sent into a spectrum analyzer to do beat frequency. The APD (Hamamatsu company, S2381) is made from silicon. Its response bandwidth is about 2 GHz for 400-1000 nm wavelength.

The concept of eliminating the modulation process on the Nd:YAG 1 laser is to offer the same amplitude and out phase signal (compared to original modulation signal) to eliminate the original modulation signal. Therefore, we first give phase lock on function generator 3 and 2. We also use the FG 3 to input a sine wave of 147 mV, 30 kHz into the frequency stabilization control system for the Nd:YAG 1 laser. The 532 nm beam is modulated. Then we simultaneously offer a sine wave of 200 mV, 30 kHz from the FG 2 and a DC voltage from the FG 1 to the radio frequency driver. At beginning, we both tune the FG 2 and the FG 3 and make them have the same phase. And then we try to change the amplitude size of the sine wave from the FG 2 and the phase difference between the FG 2 and the FG 3. We also simultaneously observe the change of the beat frequency signal from the spectrum analyzer. The smallest beat frequency signal we have obtained is shown in Fig. 3.6. We have successfully reduce the modulation effect on the Nd:YAG 1 laser. The observed signal is fitted with Gaussion profile and the fitted FWHM linewidth is about 180 kHz. Although the 532 nm laser beam after the double-passed AOM frequency shifter still has a broadened linewidth of 180 kHz than original linewidth of 5 kHz, it is smaller than the a_{10} linewidth and we can use it to measure the a_{10} linewidth.

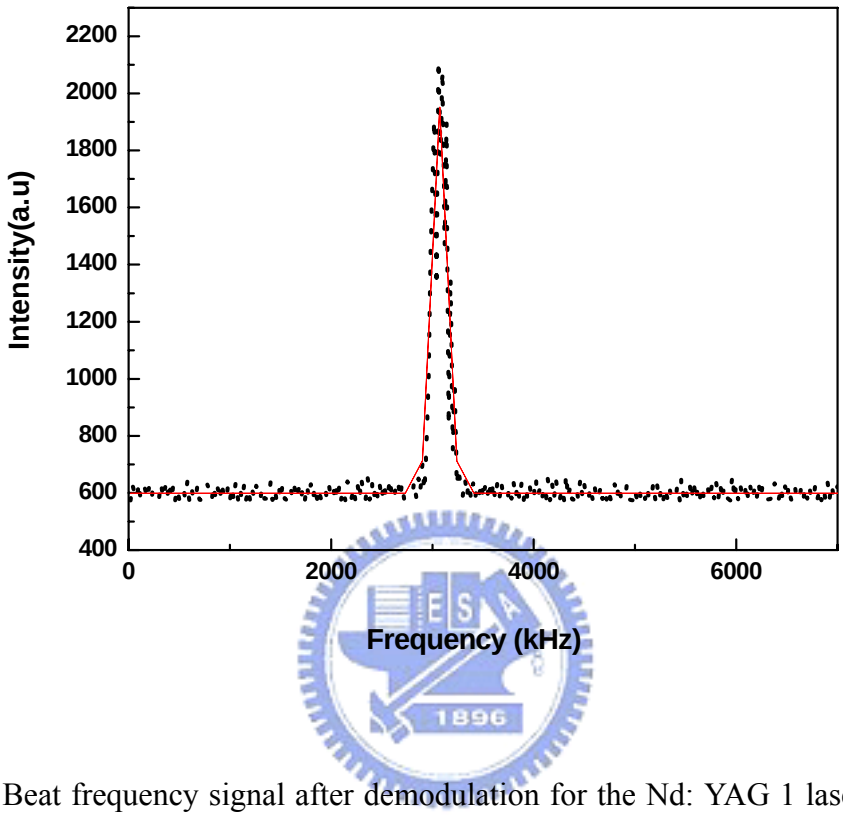

Fig. 3.6. Beat frequency signal after demodulation for the Nd: YAG 1 laser. The solid line is the fitted Gaussion profile. The fitted FWHM width is about 180 kHz.

Figure 3.7 shows the saturation spectrum of the a_{10} component. For comparison, we carefully adjust the intensities of the pump and probe beams (See Fig. 3.4.) such that they equal to the intensities used in PAM. The observed saturation spectrum is fitted with Lorentzian profile and the fitted FWHM linewidth is 1.952±0.018 MHz. The observed lineshape shows a little asymmetric. It is probably due to the non-constant background. It requires further study in the future. Because the 532 nm laser beam after the double-passed AOM frequency shifter has a linewidth of 0.18 MHz. Therefore, the FWHM linewidth of the a_{10} component is 1.772 MHz (i.e. 1.952－0.18 MHz) [6,7]. This value is in agreement with the linewidth of 1.755 MHz using PAM within the uncertainty.

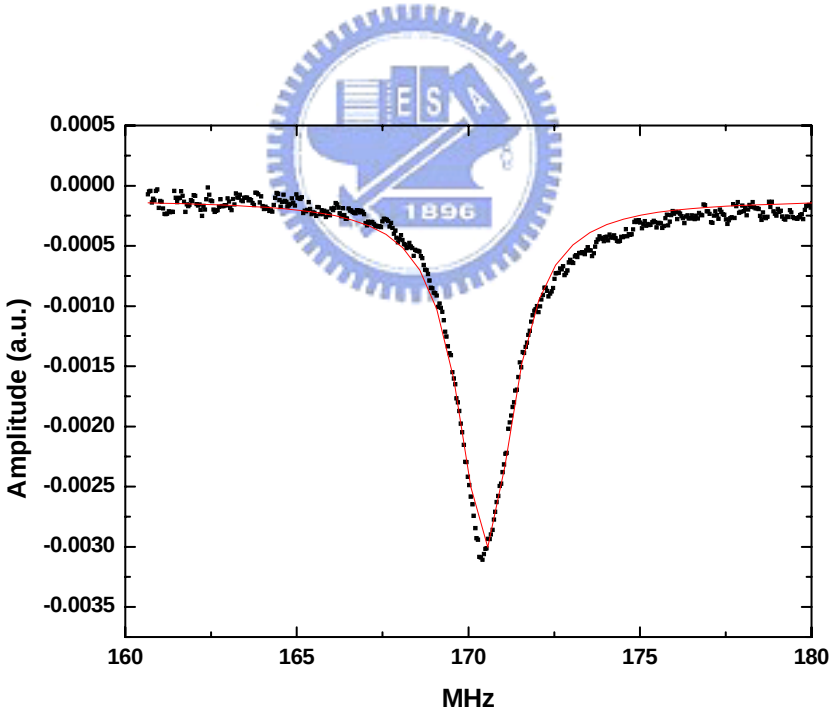

Fig. 3.7. Saturation spectrum of the a_{10} component. The solid line is the fitted Lorentzian profile. The fitted FWHM width is 1.952±0.018 MHz.

3.3.2 Pressure Broadening

After verifying the PAM method for linewidth determination, we use it to investigate the variation of the linewidth of a_{10} with respect to the laser power and the vapor pressure of iodine. To investigate the variation of the linewidth with respect to vapor pressure of the iodine cell, we fix the pump power at 4.75 mW and vary the cold finger temperature of the iodine cell from -8.32 ^{o}C (vapor pressure = 1.74 Pa) to 10 ^{o}C (vapor pressure = 10.86 Pa). The variation of the a_{10} linewidth with iodine vapor pressure is shown in Fig. 3.8. The FWHM linewidth varies from 1.657 to 2.219 MHz. The slope of the linear fit is 63±2 kHz/Pa for FWHM linewidth. For comparison, pressure broadening is 106 kHz/Pa for the b_{15} component of P(48) 11-3 transition [8] and is 148 kHz/Pa for the a_1 component of R(56) 32-0 transition [9].

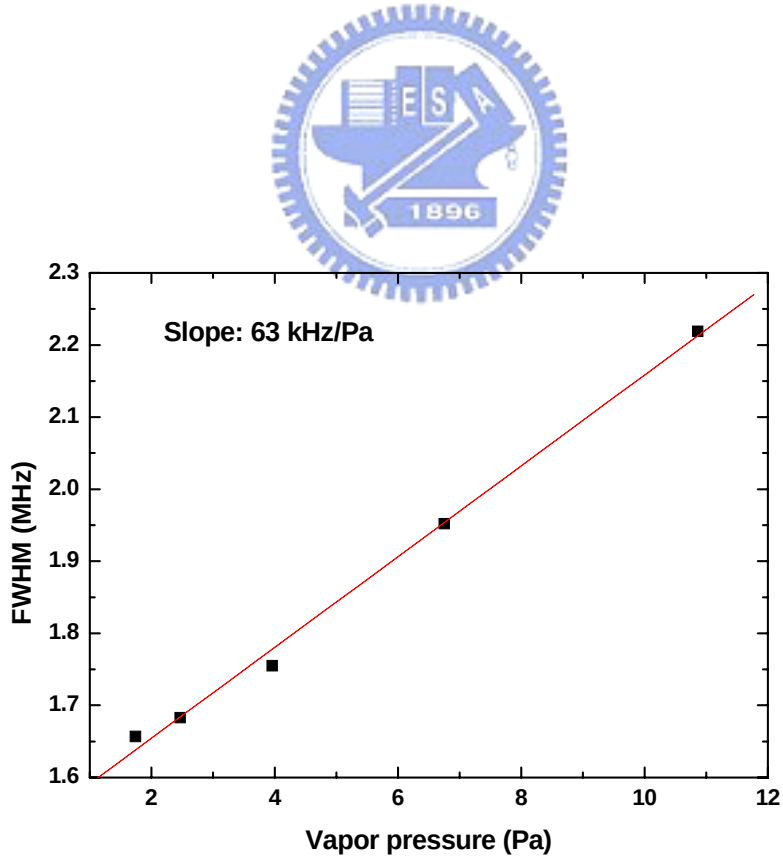

Fig. 3.8. The a_{10} linewidth vs. vapor pressure of the iodine cell. The pump power is fixed at 4.75 mW. The pressure broadened linewidth is quite linear with a slope of 63±2 kHz/Pa.

3.3.3 Power Broadening

To investigate the variation of the linewidth due to laser power, we adjust pump power from 0.19 mW to 4.75 mW and fix cold finger temperature of the iodine cell at -0.58 ^{o}C (vapor pressure = 3.9 Pa). The probe power is 27 % of the pump power. The variation of the a_{10} linewidth with pump power is shown in Fig. 3.9. The FWHM linewidth increases from 1.482 to 1.690 MHz. The linewidth and pump power have following relation [9,10]

$$\gamma' = \gamma(1+\sqrt{(1+P/P_S)}) \qquad (21)$$

here, γ is the FWHM linewidth associated with the limit of weak saturating and probe beams, P is the pump power, and P_S is the saturating power. Using a nonlinear least-squares fit to the data shown in Fig. 3.9, we obtain that γ is 0.74 MHz and P_S is 7.65 mW. Since the diameter of the pump beam in the center of the iodine cell is about 1.3 mm, the saturation intensity is about 5.76 mW/ mm^2. For comparison, the FWHM linewidth of the a_1 component of R(56) 32-0 transition is 0.288 MHz at the vapor pressure of 1.4 Pa and its pressure broadening is 148 kHz/Pa [9]. Consequently, the a_1 linewidth at the vapor pressure of 3.9 Pa is about 0.66 MHz. Our fitted a_{10} linewidth of 0.74 MHz at 3.9 Pa is close to it.

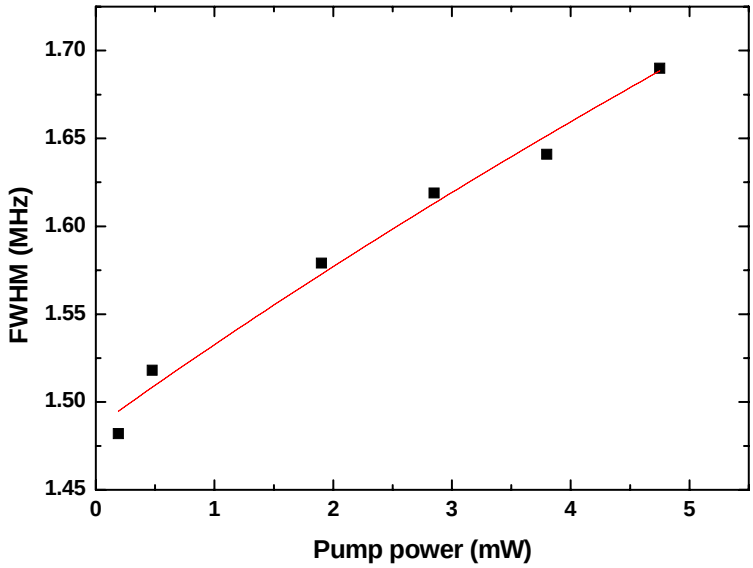

Fig. 3.9. The a_{10} linewidth vs. pump power. The cold finger temperature of the iodine cell is fixed at -0.58 ^{o}C (vapor pressure = 3.9 Pa). The fitted results are γ = 0.74±0.007 MHz and P_s = 7.65±0.56 mW.

3.4 Conclusions

We have verified that the Lorentzian linewidth can be easily determined by using the dependence of the peak amplitude of the third-derivative signal on the modulation width (PAM). We have also used this method to investigate pressure broadening and power broadening of the a_{10} component of R(56) 32-0 transition of $^{127}I_2$ at 532 nm systematically. The pressure broadened linewidth is quite linear with vapor pressure. The slope of the linear fit is 63 kHz/Pa for FWHM width. From the power broadening parameter the saturation intensity is obtained to be 5.76 mW/mm^2.

References

[1] A. Arie, S. Schiller, E. K. Gustafson, and R. L. Byer, Opt. Lett. **17**, 1204 (1992).

[2] A. Arie and R. L. Byer, J. Opt. Soc. Am. B **10**, 1990 (1993).

[3] J. L Hall, L.-S. Ma, M. Taubman, B. Tiemann, F.-L. Hong, O. Pfister, and J. Ye, IEEE Trans. Instrum. Meas. **48**, 583 (1999).

[4] T. J. Quinn, Metrologia **40**, 103 (2003).

[5] K. Nyholm, M. Merimaa, T. Ahola, and A. Lassila, IEEE Trans. Instrum. Meas. **52**, 284 (2003).

[6] J. H. Eberly, Phys. Rev. Lett. **37**, 1387 (1976).

[7] A. T. Georges and P. Lambropoulos, Phys. Rev. A **18**, 587 (1978).

[8] M. Gläser, Metrologia **23**, 45 (1986).

[9] M. L. Eickhoff and J. L. Hall, IEEE Trans. Instrum. Meas. **44**, 155 (1995).

[10] V. S. Letokhov and V. P. Chebotayev, Nonlinear laser spectroscopy, Berlin, Springer-Verlag, 72 (1977).

Chapter 4

Measurement of Hyperfine Splitting by Using Double-Passed Acousto-Optic Modulator Frequency Shifter

4.1 Research Motivation

I_2 has always been an attractive subject for spectroscopy because of its rich spectra from the UV to the IR. The HFS components of I_2 spectra have also shown to be suitable frequency references for laser frequency stabilization (see references in [1]). Moreover, I_2 also provides a good subject with which to test theoretical models for Hamiltonian of hyperfine interactions [2]. For these interactions, the measured hyperfine splittings are fitted to a four-term Hamiltonian and the corresponding hyperfine constants could be obtained.

In general, the hyperfine splitting is measured by heterodyne technique. Two lasers are independently stabilized to different hyperfine components and their frequency difference is obtained by measuring their beat frequency. However, not every laboratory could set up two iodine-stabilized lasers for measuring hyperfine splitting due to the budget or the commercial availability of laser. For example, we have observed the hyperfine structures for sixteen iodine transitions at 531 nm using a frequency doubled 1062 nm alpha-distributed feedback diode laser [3]. Since the alpha-distributed feedback diode laser is discontinued by the manufacturer, we are not able to set up second laser and measure the hyperfine splitting using the heterodyne technique.

To solve this problem, we use a double-passed acousto-optic modulator (AOM) frequency shifter to measure the hyperfine splitting of the iodine. The frequency shifting property of the AOM has been widely used in laser frequency stabilization [2] and laser spectroscopy [4]. However, laser frequency is stabilized to the molecular transition and the result which measured another transition by the double-passed AOM frequency shifter is seldom reported until now. Moreover, the method is inexpensive and easily set up.

Consequently we use the method to replace heterodyne technique.

In this chapter, we present our measurement results of the hyperfine splittings of R(56) 32-0 transition of $^{127}I_2$ using a double-passed AOM frequency shifter similar to the arrangement in ref. 4. The hyperfine splittings of iodine lines near 532 nm have also been measured precisely by heterodyne technique using two iodine-stabilized lasers [5,6]. Our measurement results will compare with the values recommended by Consultative Committee for Length (CCL) [1].

4.2 Experimental Setup

The experimental setup is shown in Fig. 4.1. The experimental setup consists of three parts: laser frequency stabilization, AOM frequency shifter, and saturation spectroscopy of iodine.

We use the same NPRO Nd:YAG laser (It is described in **3.3** of Chapter 3) as the light source.

The laser frequency is modulated at 30 kHz with a width of 1.5 MHz. The laser beam passes through a 30 dB Faraday Isolator to prevent the optical feedback effect and then is focused into a PPLN crystal (It is also described in **3.3** of Chapter 3). The λ/2 is used to adjust the light polarization to match the PPLN z-direction. We divide the 532 nm second-harmonic light into two beams using a beam splitter (BS). The power of one beam is 1.5 mW and the other beam is 6.5 mW.

We use the 1.5 mW laser beam to lock the laser to one hyperfine component of R(56) 32-0 transition. This laser beam enters a 10-cm long iodine cell as the pump beam after passing a polarizing beam splitter (PBS) and a quarter wave plate (λ/4). The pump beam is collimated to 1.3 mm in diameter at the center of the I_2 cell. The cold finger of the iodine cell is kept at 0 ^{o}C (corresponding to iodine vapor pressure of 4.1 Pa). A fraction of the pump beam reflected by a partial reflection mirror (PRM) is detected by a photodiode (PD). The Doppler-free saturation spectrum of the hyperfine components of R(56) 32-0 transition is observed and recorded using the conventional third-harmonic demodulation method by a lock-in amplifier. The time constant of the lock-in amplifier is 30 ms. In order to stabilize the Nd:YAG laser, the third-harmonic output of the lock-in amplifier is fed into the thermal tuning via a servo control loop.

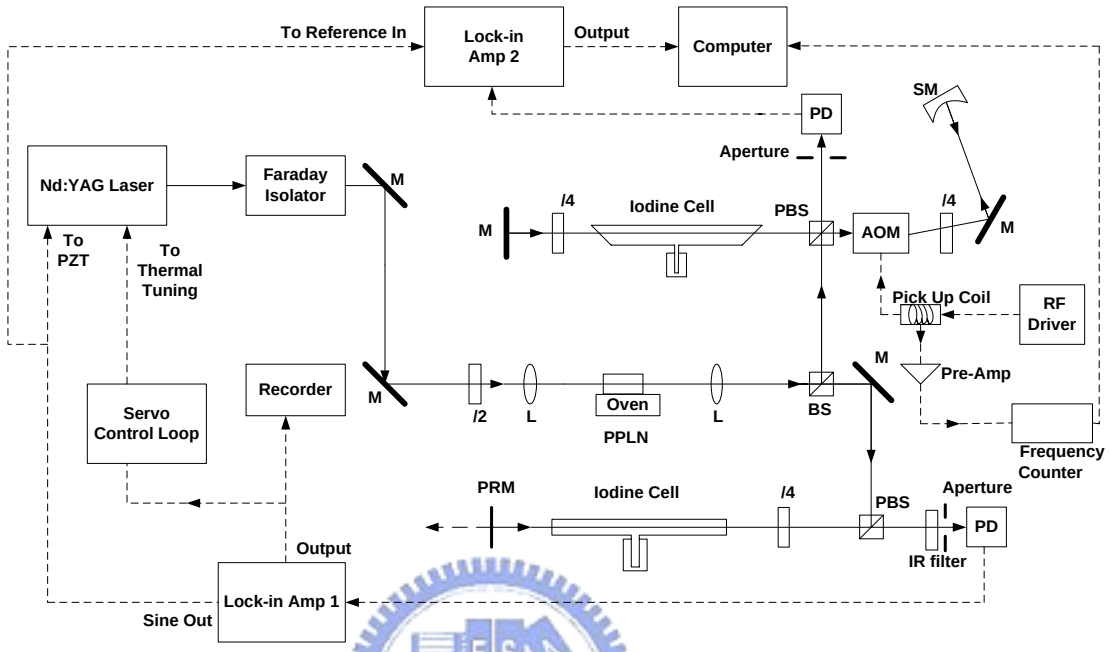

Fig. 4.1. Experimental setup for measuring hyperfine splitting of molecular iodine using a double-passed acousto-optic modulator frequency shifter. M, mirror; λ/2, half wave plate; L, lens; PPLN, periodically poled $LiNbO_3$; BS, beam splitter; PBS, polarizing beam splitter; λ/4, quarter wave plate; PRM, partial reflection mirror; PD, photodiode; AOM, acousto-optic modulator; RF, radio frequency; Pre-Amp, pre-amplifier; SM, spherical mirror (concave).

λ

The 6.5 mW laser beam enters an AOM (Isomet, Modulator: 1205C, Driver: D301B) to generate a frequency tunable beam for the saturation spectroscopy of the hyperfine components of R(56) 32-0 transition. The detail working principle of the double-passed frequency shifter has been described in ref. 4. The frequency of the light diffracted by the AOM is changed by the amount pf_{AOM} where p (positive or negative integer) is the diffraction order and f_{AOM} is the AOM carrier frequency.

We use a function generator (HP 33120A) to offer DC voltage to control the radio frequency (RF) driver (Every time changes 0.1 mV, corresponding to 350 Hz). The variable-frequency RF driver allows the carrier frequency to be varied from 57 to 103 MHz. The relationship between carrier frequency and DC voltage is shown in Fig. 4.2. To check the stability of the carrier frequency of the AOM, we input 10 V_{dc} to control the RF driver and observe the drift of the carrier frequency up to 20 minutes. The frequency drift is smaller than 3.25 kHz in 20 minutes. The stability of the carrier frequency of the AOM is 4.06×10^{-5} and is shown in Fig. 4.3. A frequency counter (HP 5316B) monitors the output of the RF driver and measures the carrier frequency through a pick-up coil. Because the signal of the RF driver is very small, we amplify it by using a pre-amplifier. To confirm the accuracy of the frequency reading for the HP counter, we also simultaneously send the signal of the RF driver into a spectrum analyzer. The frequency reading of the HP counter is consistent with the spectrum analyzer.

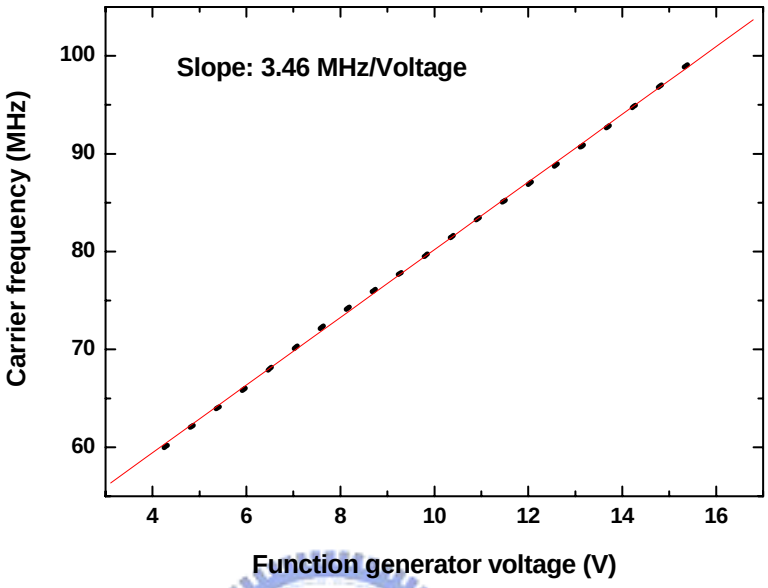

Fig. 4.2. Carrier frequency v.s. DC voltage. The solid line is the fitted Linear profile. The fitted slope is 3.46 MHz/Voltage.

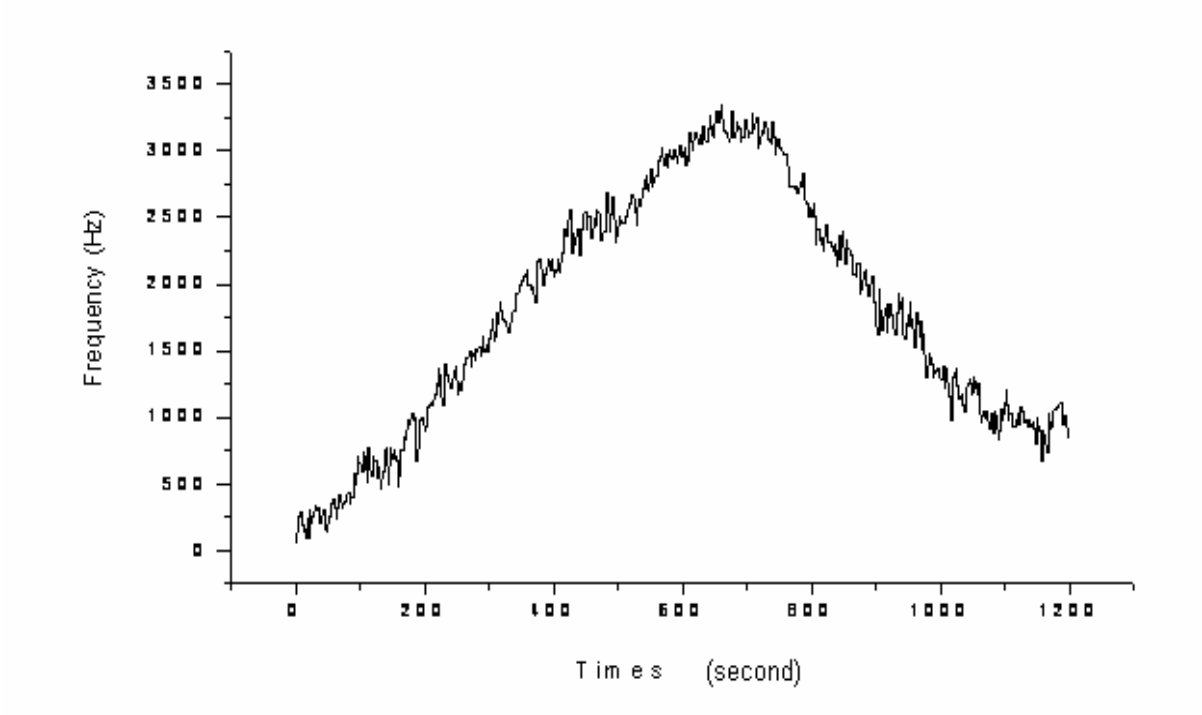

Fig. 4.3. Stability of the carrier frequency of the AOM is 4.06×10^{-5}. The frequency drift is smaller than 3.25 kHz in 20 minutes.

When the 532 nm laser beam first passes through the AOM, one of the diffracted beams is selected. After the AOM, a quarter wave plate (λ/4) converts the diffracted beam from the linear to circular polarization state. Next, the spherical mirror retro-reflects the diffracted beam passing through both the λ/4 plate and the AOM. The second pass through the λ/4 plate yields a linearly polarized beam with a polarization plane orthogonal to that of the input beam, allowing the PBS to separate the input beam and the double-diffracted beam. The input beam doubly passes through the AOM and finally is formed with the twice-diffracted beam. We name such system as a double-passed AOM frequency shifter. One should note that the diffracted angle of a diffracted beam changes according to carrier frequency but the double-passed AOM frequency shifter does not have this trouble. The optical beam entering the double-passed AOM frequency shifter finally returns to the originally optical path as going out from the AOM frequency shifter. To optimize the AOM diffraction efficiency for the twice-diffracted beam, the beam curvature at the spherical mirror is matched to the mirror curvature radius of 60 cm. For the first-order diffracted beam, the twice-diffracted conversion efficiency is between 15 and 23 % shown in Fig. 4.4, and the frequency shift is between 114 and 206 MHz. For the second-order diffracted beam, the conversion efficiency is smaller than 5 % and the twice-diffracted frequency shift is between 228 and 412 MHz.

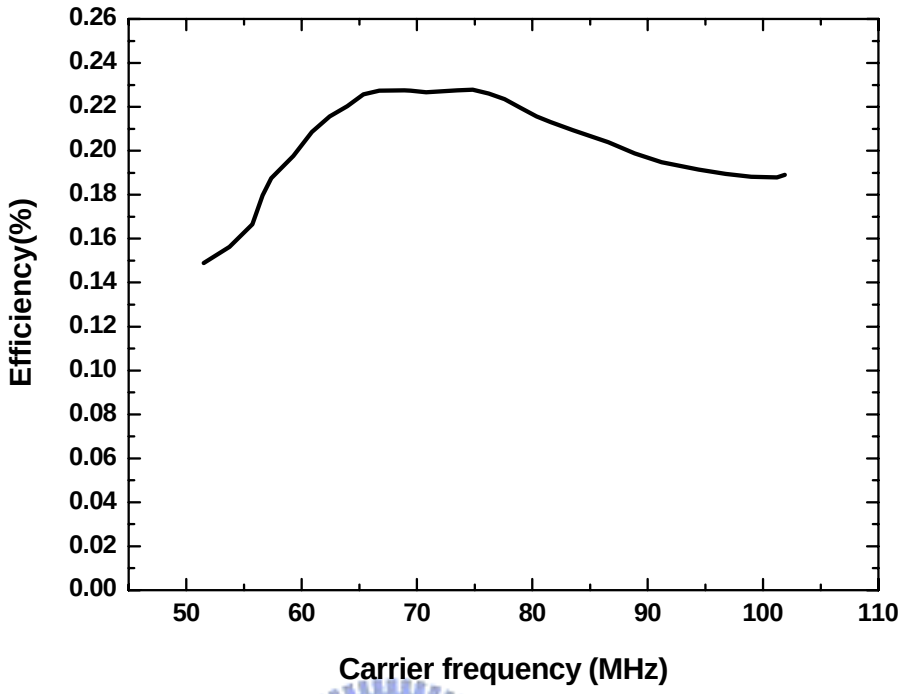

Fig. 4.4. Twice-diffracted conversion efficiency for the first-order diffracted beam. It is between 15 and 23 %.

Finally, we use the 532 nm laser beam out of the double-passed AOM frequency shifter to observe the saturation spectrum of a hyperfine structure. It enters a 10-cm long iodine cell with Brewster windows. The beam size is about 2 mm in diameter at the center of the cell. Its cold finger is also kept at 0 ^{o}C. An arrangement similar to frequency stabilization of the Nd:YAG laser is employed. The third-derivative signal of the saturation spectrum of hyperfine component of R(56) 32-0 transition is observed by a lock-in amplifier and recorded by a computer. By adjusting the carrier frequency using the RF driver, we tune the frequency of the 532 nm laser beam and scan the hyperfine component. Consequently we measure the hyperfine splitting.

4.3 Results and Discussion

First, we lock the Nd:YAG laser to the a_{10} component of R(56) 32-0 transition and scan the a_6-a_9 and the a_{11}-a_{14} components using the AOM frequency shifter. For the components a_2, a_3, a_4, a_5, and a_{15}, we lock the Nd:YAG laser to one component and scan the component within the tuning range of first-order diffracted beam. The frequency stability of the Nd:YAG laser is about 20 kHz. Figure 4.5 shows the result in which we lock the Nd:YAG laser to the a_{10} component and scan the a_6 component. The frequency interval between the a_{10} and the a_6 component is 170 066 kHz determined by a linear fitting to the portion near the center. Figure 4.6 shows the result in which we lock the Nd:YAG laser to the a_6 component and scan the a_2 component. The frequency interval between the a_6 and the a_2 component is 141 789 kHz determined by a linear fitting to the portion near the center. The frequency interval between the a_1 and the a_2 component is about 260 MHz so we lock the Nd:YAG laser to the a_2 component and scan the a_1 component using the -2nd order diffracted beam of the AOM.

The measured hyperfine splitting are listed in Table I. Using the a_{10} component as reference, the hyperfine splitting of R(56) 32-0 transition determined from our measurements are listed in Table Π. The differences of the hyperfine splitting between our results and CCL (1.5 kHz uncertainty) are also presented in the Table I and Π. The discrepancy is below 20 kHz. The main contribution to the discrepancy is the frequency stability since we make only one measurement for each splitting (except a_{10}-a_{11}, see below) listed in Table I. The frequency stability estimated from the error signal after laser is locked is less than 20 kHz. The other contributions include pressure shift and impurities in different iodine cells, and different experimental conditions for frequency locking and saturation spectroscopy.

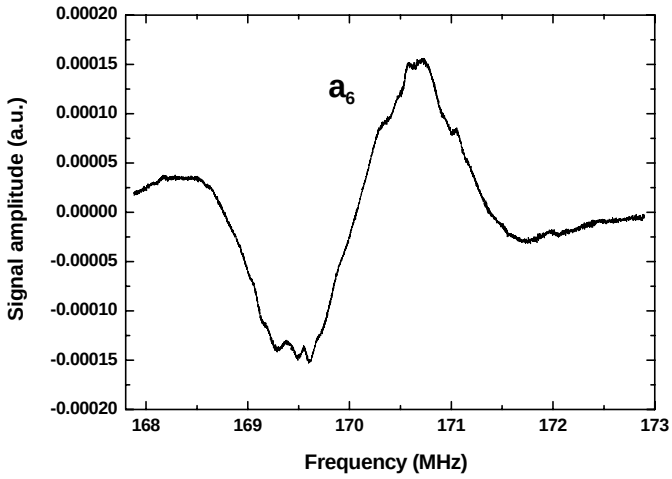

Fig. 4.5. Third-derivative saturation spectrum of a_6 component of R(56) 32-0 transition. We lock the Nd:YAG laser to the a_{10} component and scan the a_6 component using the acousto-optic modulator frequency shifter. The frequency interval between the a_{10} and the a_6 component is 170 066 kHz.

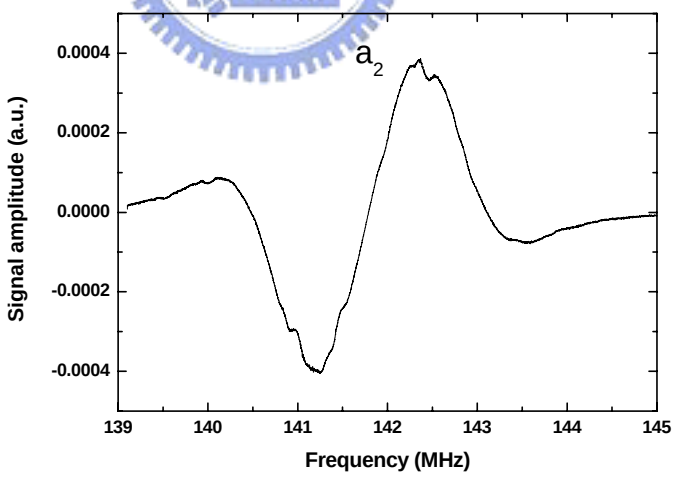

Fig. 4.6. Third-derivative saturation spectrum of a_2 component of R(56) 32-0 transition. We lock the Nd:YAG laser to the a_6 component and scan the a_2 component using the acousto-optic modulator frequency shifter. The frequency interval between the a_6 and the a_2 component is 141 789 kHz.

Table I. Measured hyperfine splitting of R(56) 32-0 transition

Hyperfine Splitting	Measured (MHz)	CCL[a] (MHz)	Meas.-CCL (kHz)
$a_1 \sim a_2$	259.701	259.698	3
$a_2 \sim a_6$	141.789	141.780	9
$a_3, a_4 \sim a_7$	131.128	---	---
$a_5 \sim a_9$	143.990	143.977	13
$a_6 \sim a_{10}$	170.066	170.064	2
$a_7 \sim a_{10}$	154.547	154.548	- 1
$a_8 \sim a_{10}$	131.930	131.916	14
$a_9 \sim a_{10}$	116.202	116.199	3
$a_{10} \sim a_{11}$	126.510	126.513	- 3
$a_{10} \sim a_{12}$	131.223	131.212	11
$a_{10} \sim a_{13}$	154.503	154.488	15
$a_{10} \sim a_{14}$	160.682	160.665	17
$a_{14} \sim a_{15}$	125.747	125.747	0

[a]CCL is Consultative Committee for Length.

Table Π. Measured hyperfine splitting of R(56) 32-0 transition using the a_{10} component as a reference

Hyperfine Splitting	Measured (MHz)	CCL (MHz)	Meas.-CCL (kHz)
a_1	-571.556	-571.542	-14
a_2	-311.855	-311.844	-11
a_3, a_4	-285.675	---	---
a_5	-260.192	-260.176	-16
a_6	-170.066	-170.064	-2
a_7	-154.547	-154.548	+ 1
a_8	-131.930	-131.916	-14
a_9	-116.202	-116.199	- 3
a_{10}	0	0	0
a_{11}	126.510	126.513	- 3
a_{12}	131.223	131.212	11
a_{13}	154. 503	154.488	15
a_{14}	160.682	160.665	17
a_{15}	286.429	286.412	17

To check the precision and accuracy, we lock the Nd:YAG laser to the a_{10} component and repeatedly scan the a_{11} component fifteen times. The result is shown in Fig. 4.7. The fifteen measured hyperfine splitting is averaged to 126.508 MHz with a standard deviation of 5 kHz. This value is comparable with CCL value (126.513 MHz). The difference is only 5 kHz.

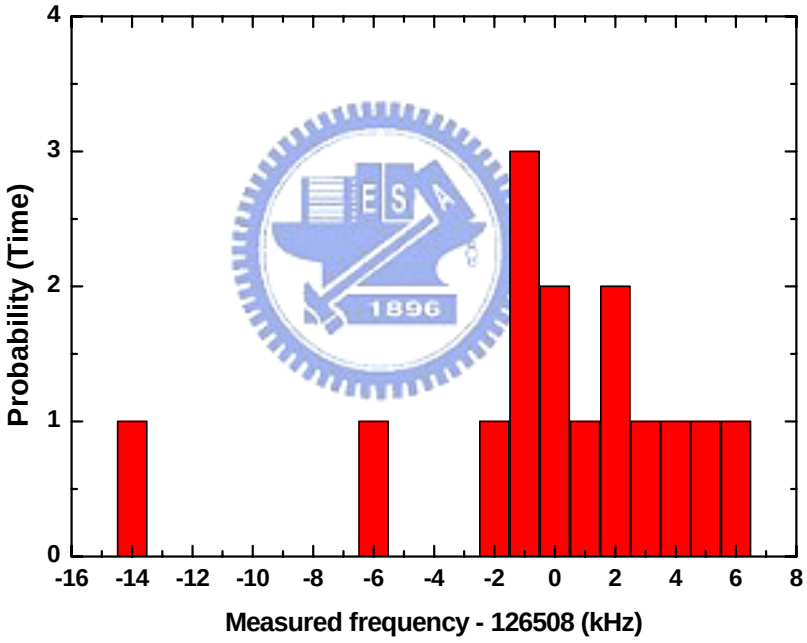

Fig. 4.7. Hyperfine splitting between the a_{10} component and the a_{11} component. We lock the Nd:YAG laser to the a_{10} component and repeatedly scan the a_{11} component 15 times.

Usually there is an offset between two lasers locked to same hyperfine component due to different cells, different operation conditions, and offset in servo electronics. To eliminate this offset in the hyperfine splitting measurement, in the conventional heterodyne technique, the hyperfine splitting is determined by measuring the beat frequencies of all hyperfine components with respect to a second stabilized laser first and the hyperfine splitting is then obtained by simple subtraction. Since the span of the hyperfine components is about 1 GHz, we are not able to measure the hyperfine splitting of all components with respect a selected component. For example, the hyperfine splitting of a_1 component to a_{10} component is obtained by adding the results of three different measurements. It will of course have larger uncertainty. Besides, we are not able to remove the offset mentioned in above. There are two other disadvantages of our method compared to heterodyne technique: 1. larger laser power is required; 2. diffracted beam power changed with AOM carrier frequency. The first may limit the application of our method and the second can be solved by intensity stabilization.

We will improve the accuracy of our method in the near future. For example, we can lock the voltage controlled oscillator of the RF driver to the measured hyperfine peak and measure the frequency more carefully. To reduce the error from pressure shift and impurities in different cells we have made a special cell in which two cells are connected by a tube. We will also try to reduce the offset of the servo electronics by better circuit design.

4.4 Conclusions

We have measured the hyperfine splitting of R(56) 32-0 transition of molecular iodine at 532 nm using a double-passed AOM frequency shifter. Preliminary results, compared with the values recommended by the Consultative Committee for Length, show accuracy better than 20 kHz and it can be easily improved. In the future we will improve the accuracy of this method and use it to measure the hyperfine splittings of the iodine lines at 531 nm observed by our alpha-distributed feedback laser.

References

[1] T. J. Quinn, Metrologia **40**, 103 (2003).

[2] For example, L.-S. Chen, W. Y. Cheng and J. Ye, J. Opt. Soc. Am. B **21**, 820 (2004).

[3] T.-L. Huang, W.-Y. Cheng, Y.-R. Lin, J.-T. Shy and H.-P. Liu, Jap. J. Appl. Phys. **39**, L559 (2000).

[4] For example, J. T. Hodges, H .P. Layer, W. W. Miller and G. E. Scace, Rev. Sci. Instrum. **75**, 849 (2004).

[5] A. Arie and R. L. Byer, J. Opt. Soc. Am. B **10**, 1990 (1993).

[6] F.-L. Hong, J. Ye, L.-S. Ma, S. Picard, C. J. Bordé and J. L Hall, J. Opt. Soc. Am. B **18**, 379 (2001).

Chapter 5

Frequency Stabilization of an External Cavity Diode Laser to Molecular Iodine

5.1 Research Motivation

Except for the diode-pumped, frequency doubled Nd:YAG laser at 532 nm we study in Chapter 3, we are also interesting in using diode lasers for frequency stabilization. For diode lasers, their smaller size, larger tuning range, higher power, and compactness make them an attractive source for frequency stabilization. Frequency stabilization of the external cavity diode laser (ECDL) to the iodine HFS components using extra-cavity iodine cell has been extensively studied and reported at 633 nm [1-4], 637 nm [5-6], and 657 nm [7].

In the past, the dominant optical frequency standard has been He-Ne laser stabilized to iodine at 633 nm. Most member states of the Convention du Mètre have adopted such lasers as the national realization of the meter. Frequency uncertainty of ± 10 kHz is regularly achieved [8]. However, the output power of a He-Ne laser is low and He-Ne lasers are large in size and mechanically vulnerable. There is thus growing interest in using diode lasers for frequency stabilization.

A portable laser frequency standard at 633 nm has been constructed by frequency stabilizing a miniaturized ECDL [4]. Its frequency stability matches that of iodine-stabilized He-Ne lasers at 633 nm. The best stability, 1×10^{-13}, is reached at an integration time of 4000 s. The systems in Ref. 1-7 use the traditional third-harmonic locking technique. The frequency modulation is achieved by modulating the cavity length of the ECDL using a piezoelectric transducer. This modulation scheme limits the modulation frequency to <10 kHz. The frequency of ECDL can be also modulated by modulating current through the diode. The current modulation allows modulation frequency higher than PZT modulation for an ECDL. To reduce the noise, we choose to modulate the laser frequency by modulating the diode

current instead of the cavity length by PZT.

The reasons we choose P(84) 5-5 transition of $^{127}I_2$ at 657.483 nm for our study are as follows. First, the $^1S_0$-$^3P_1$ intercombination line of Ca at 657.459 nm has a linewidth much narrower than the HFS components of iodine. It is a useful reference for a precise optical frequency standard. Recently we have developed a novel Ca absorption cell and successfully observed its saturation absorption spectrum with a linewidth below 300 kHz [9]. To further investigate the high resolution spectroscopy of the Ca, we want to develop a stable diode laser system at 657 nm as a stable light source. Second, the diode laser at 657 nm has the characteristics of lower cost and higher power than diode laser at 633 nm. It is an attractive alternative for red diode laser systems locked to iodine. Therefore, we decide to investigate the saturation spectrum of the hyperfine components of P(84) 5-5 transition of $^{127}I_2$ at 657.483 nm (~ 17 GHz away from the Ca transition) for frequency stabilization of our ECDL laser.

5.1.1 Literature Review

Previous works on this iodine transition are briefly reviewed here. In 1997, T. Kurosu and coworkers reported high-sensitive spectroscopy of the hyperfine components of P(84) 5-5 transition with signal-to-noise ratio (SNR) of 500 at 1 s time constant by means of power-stabilized light from a diode laser spectrometer [10]. The power-stabilized laser system is a master/slave laser system whose intensity noise was reduced by feedback stabilization. Although they obtained good SNR, they did not stabilize the laser frequency to the hyperfine component. Later, T. Masuda and coworkers reported the first frequency stabilization of a diode laser to the hyperfine component *f* of P(84) 5-5 transition [7]. Their experimental setup is complex in which the iodine cell is placed inside an external resonant cavity to increase the signal. However, the SNR is low (~ 30 at 1 s time constant) and the frequency stability is estimated to be 300 kHz.

5.1.2 Research Outline

In this chapter, we investigate the third-harmonic demodulated saturation absorption signal of the hyperfine components of P(84) 5-5 transition without using external resonant cavity to increase the signal or using power stabilization to reduce the intensity noise. We will lock the laser frequency to the hyperfine component *o* to measure frequency stability. We will also determine the linewidth of the hyperfine components of P(84) 5-5 transition using the dependence of the peak amplitude of the third-derivative signal on the modulation width (Described in Chapter 2).

5.2 Experimental Setup

Our diode laser system is shown in Fig. 5.1. The ECDL is a commercial system from EOSI. Its operation wavelength is at 657 nm. The ECDL is of the Littman-Metcalf design [11] shown in Fig. 5.2 and is composed of a laser diode, a diffraction grating and a tuning mirror. The diode laser output is collimated and is incident on the grating at a grazing angle. Its first-order beam is diffracted toward the tuning mirror. The retro-reflection off the mirror selects which wavelength is diffracted back into the diode laser. The output beam is the zero-order diffraction off the grating. The output power of the ECDL is 5.5 mW. The linewidth of the ECDL at free running is less than 1 MHz. Its frequency can be coarsely tuned by rotating the tuning mirror and finely tuned by applying a voltage to the piezoelectric transducer (PZT) attached on the grating or changing the injection current of the laser diode. To reduce environmental noises affecting the ECDL stability, we put it into an aluminum box and paste soundproof material onto the box. The soundproof material is a sound absorbing foam material containing two lead septums separated by foam. To further reduce the vibration from the table the aluminum box is placed on a layer of damping rubber.

Before investigating the iodine spectrum we first study the amplitude modulation of our ECDL induced by PZT modulation and current modulation. The PZT modulation has a resonance at 1 kHz. The amplitude modulation is 0.42 % at 30 MHz modulation width for modulation frequency less than 800 Hz. For current modulation the amplitude modulation is 0.5 % at same modulation width. We would like to emphasize that the amplitude modulation under current modulation is comparable to PZT modulation. Therefore, we choose to modulate the laser frequency by current modulation.

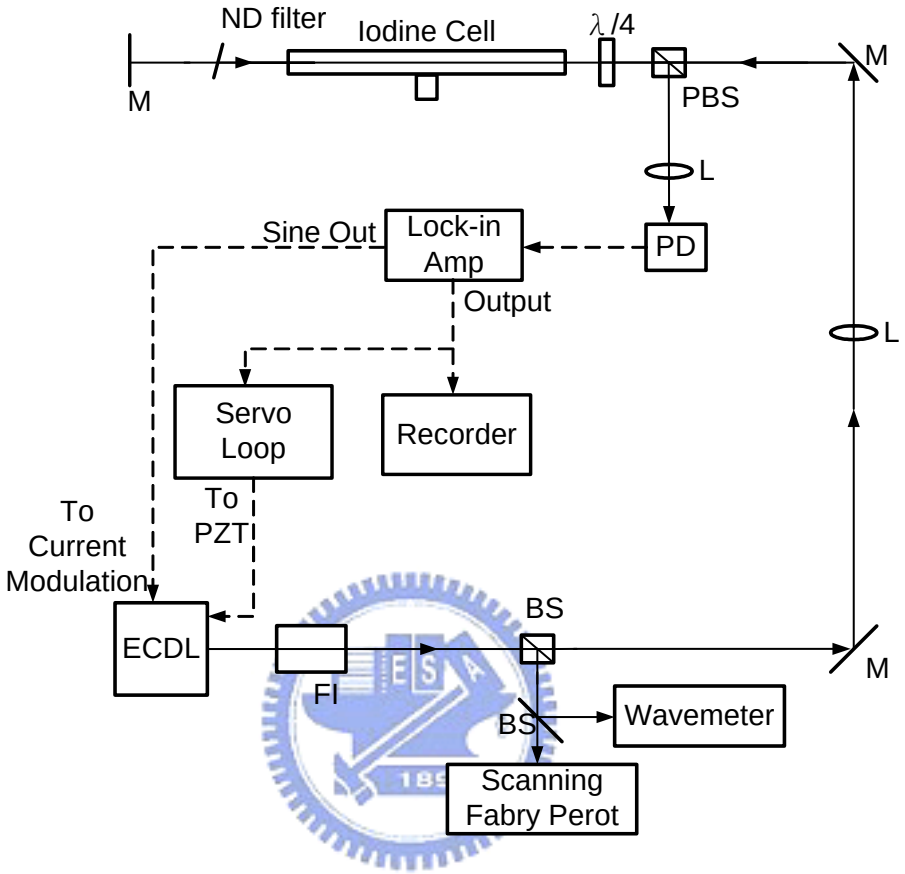

Fig. 5.1. Experimental setup. Here, ECDL-external cavity diode laser, FI-Faraday isolator, BS-beam splitter, M-mirror, L-lens, PBS-polarizing beam splitter, λ/4-quarter wave plate, ND filter-neutral density filter, PD-photodetector.

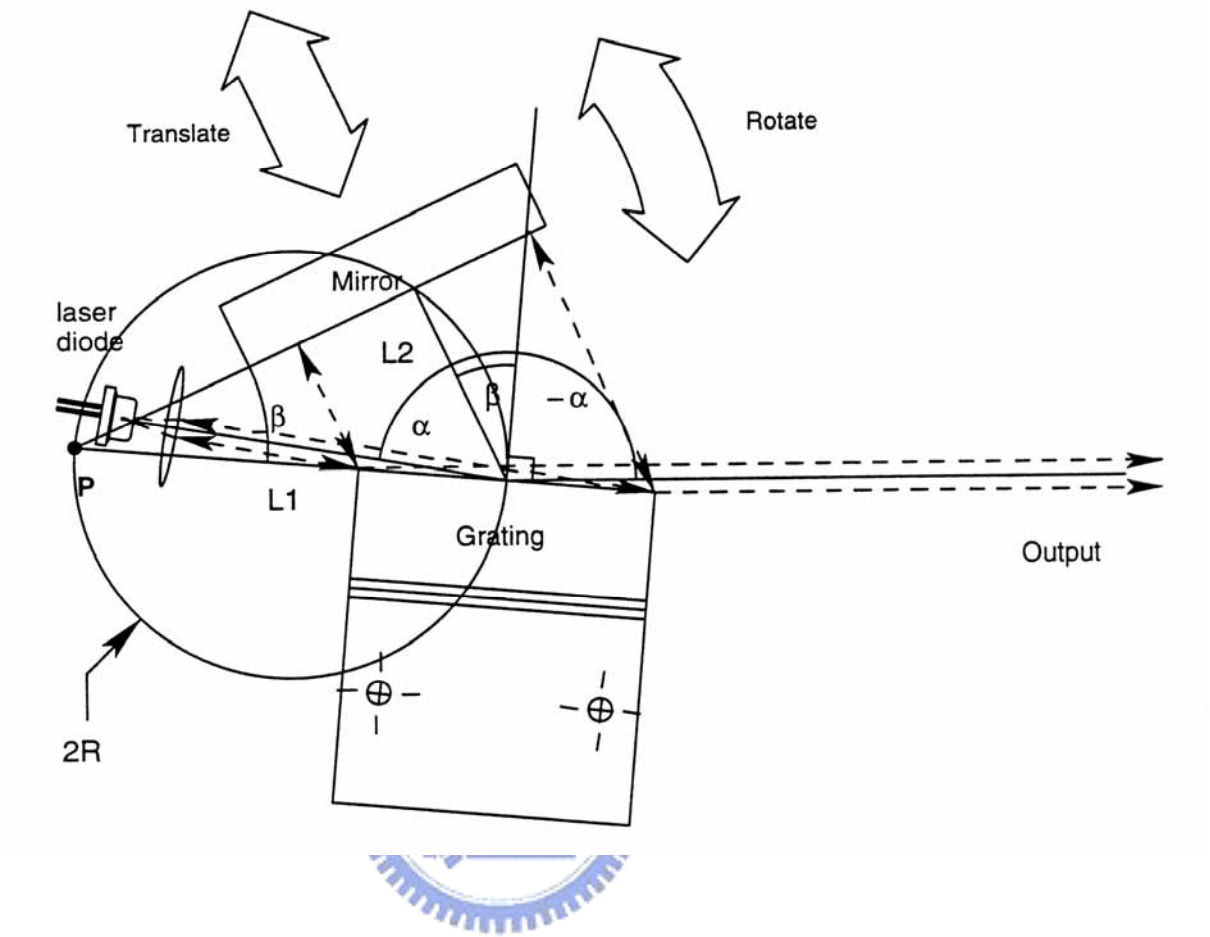

Fig. 5.2. Littman-Metcalf design of our ECDL.

The laser beam from the ECDL passes through a Faraday isolator (FI) to prevent the optical feedback effect and then it is divided into two beams by a beam splitter (BS). The weaker beam is used to monitor the laser mode and wavelength in real time by a scanning Fabry-Perot interferometer and a wavemeter, respectively. The scanning Fabry-Perot interferometer has a FSR (free spectral range) of 1.5 GHz and a finesse of > 200 and the wavemeter has an accuracy of 10^{-3} nm. The main beam is collimated to 2 mm in diameter by a lens (L) and then passes through a 60-cm iodine cell as the saturating beam with an optical power of about 3 mW. The intensity of the saturating beam is about 1 mW/mm^2. A fraction of the beam is then reflected back as a probe beam using a neutral density (ND) filter. A quarter waveplate ($\lambda/4$) and a polarizing beam splitter (PBS) are used to direct the probe beam to a photodetector (PD) and this also improves optical isolation for the ECDL. The probe beam power entering the photodetector is 0.3 mW. The cold finger temperature of the iodine cell is normally stabilized to 15 ^{o}C, resulting in an iodine vapor pressure of approximately 17 Pa.

The Doppler-free saturation spectrum of the hyperfine components of P(84) 5-5 transition is observed and recorded with the conventional third-harmonic demodulation method by a lock-in amplifier. We modulate the ECDL frequency at 15.1 kHz by modulating the laser diode injection current using the sine output of the lock-in amplifier and scan its frequency by applying a triangular signal to the PZT of the ECDL. In order to stabilize the laser frequency, the third-harmonic output of the lock-in amplifier is fed into the laser PZT via a simple one-stage integral feedback control loop.

5.3 Results and Discussion

The third-derivative signal of the saturation spectrum of the hyperfine components of P(84) 5-5 transition is shown in Fig. 5.3 in which the modulation width is 11.66 MHz. The absorption line consists of 15 hyperfine components from *a* to *o*, distributed within 1 GHz. The observed spectrum shows flat baseline with negligible offset which is important for absolute frequency stabilization. The isolated components *a*, *f*, and *o* are the best choices for frequency stabilization. The hyperfine components are obtained with a SNR of 1000 at a time constant of 1 s. Here, the SNR is the peak-to-peak amplitude of the third-derivative signal divided by the noise level. The peak-to-peak amplitude of the third-derivative signal is 10 V and the noise level is 10 mV. The present SNR is mainly limited by the detection electronics. Using our diode laser system to gain a SNR of 1000 is relatively easy. The main reasons that we can obtain such a high SNR are longer iodine cell and higher modulation frequency compared to Ref. 7 and 10. In our experiment, the iodine cell length is 60 cm compared to 25 and 20 cm in Ref. 7 and 10, and the modulation frequency is 15.1 kHz compared to 780 and 333 Hz in Ref. 7 and 10. The longer cell gives higher signal and higher modulation frequency reduces the noise. We have observed the noise size of the third-harmonic demodulated signal by an oscilloscope and we find that noise decreases as we increase the modulation frequency. Higher modulation frequency really reduces noise and improves SNR. Considering the limitation of the current driver of our ECDL we choose a modulation frequency of 15.1 kHz instead of 34 kHz set by our lock-in amplifier. The signal amplitude versus the cold finger temperature shows a maximum at about 15 ^{o}C. Therefore, in our study we keep the cold finger temperature at 15 ^{o}C.

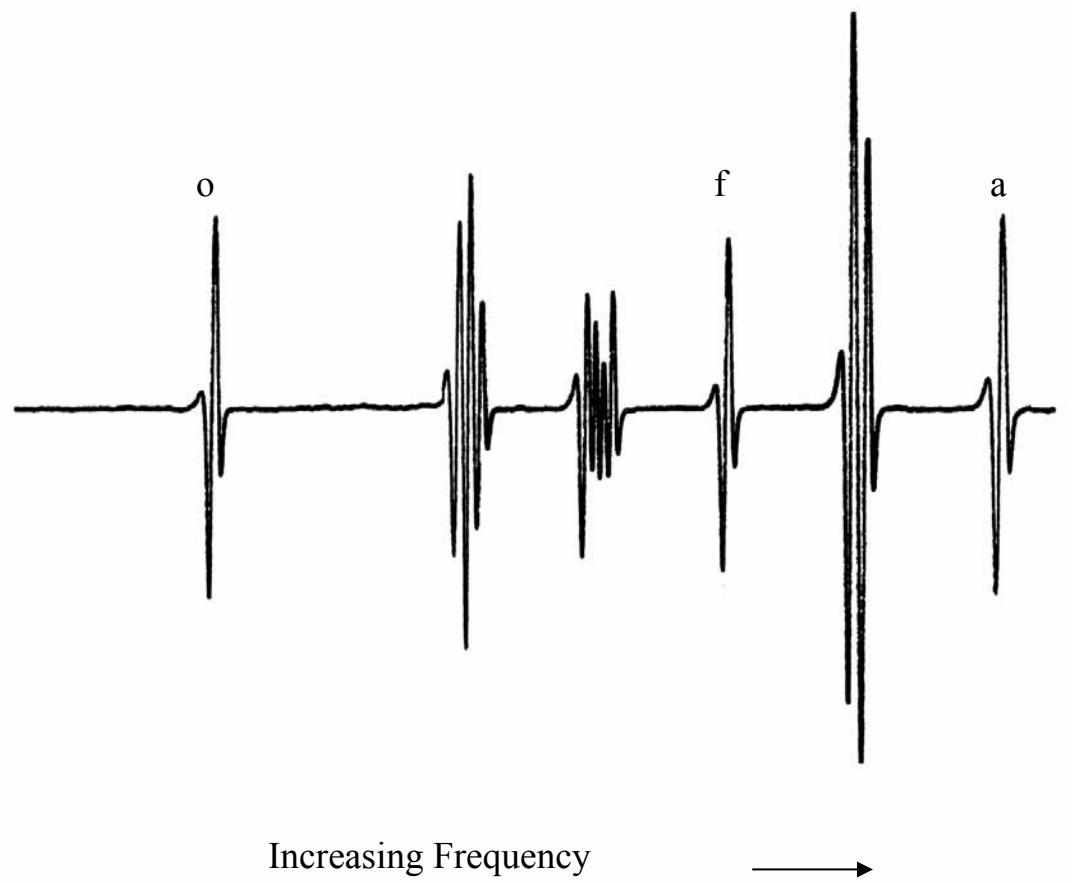

Fig. 5.3. The third-derivative signal of the saturation spectrum of the hyperfine components of P(84) 5-5 transition. Here, time constant is 1s.

In Figure 5.3, the spectrum of the 15 hyperfine components from *a* to *o* shows a little asymmetric in their lineshapes. It is a hyperfine component profile due to fast scan rate. The lineshape is symmetric while using a slower scan rate. The lineshape of the *o* component at slow scan rate is shown in Fig. 5.4.

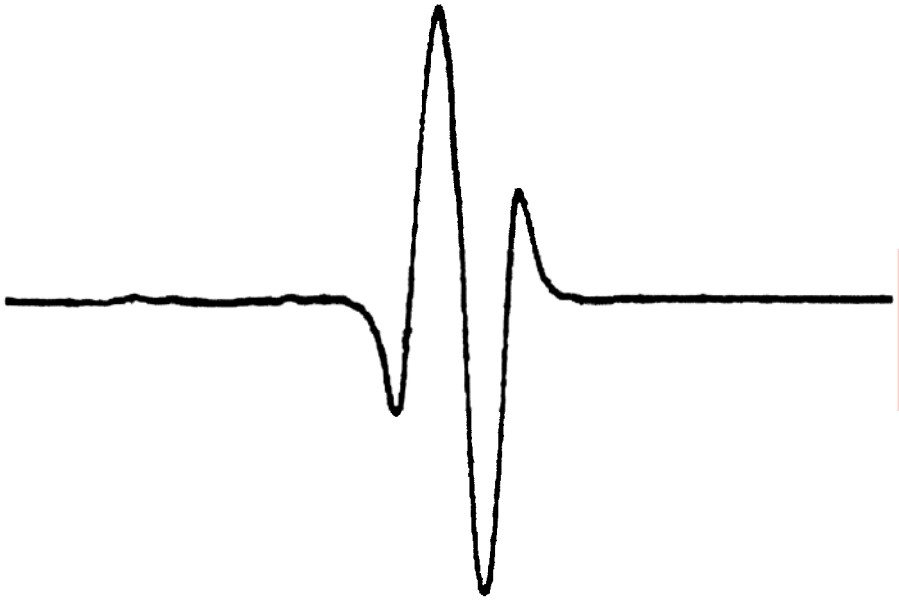

Fig. 5.4. The third-derivative signal of the *o* component using a slower scan rate.

In order to determine the linewidth of the HFS components, we use the method with the peak amplitude of the third-derivative signal on the normalized modulation width. The analytical function is as follows (We investigated in Chapter 2):

$$h(\delta_A) = (P_1\delta_A + P_2\delta_A^2 + P_3\delta_A^3)/(P_4 + P_5\delta_A + P_6\delta_A^2 + P_7\delta_A^3).$$

The peak amplitude of the third-derivative signal of HFS component *o* versus modulation width is shown in Fig. 5.5, in which the experimental result is coordinated with the fitted theoretical curve. From the fitted theoretical curve, it indicates that the measured linewidth is 7.5 MHz for HFS component *o*. The standard error is better than 0.4 MHz (or 5 %). Using this method, we have also determined the linewidth of the HFS components of *a* and *f*. Both have the same linewidth with similar standard error.

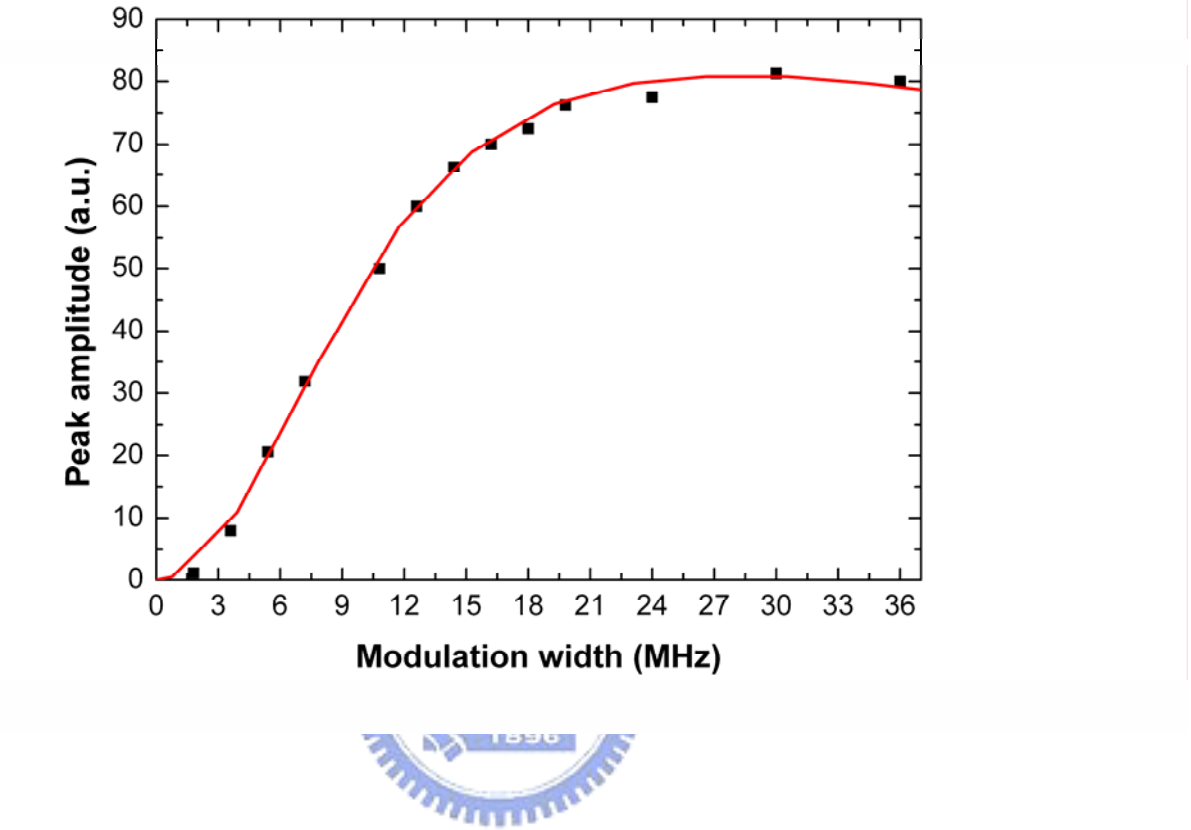

Fig. 5.5. The measured peak amplitude of the third-derivative signal as a function of modulation width (dotted points) and the theoretical fitted curve (solid line). The fitted FWHM width is 7.5±0.4 MHz.

According to Nakazawa's analysis [12], it shows that when modulation width is 1.64 times the linewidth, the third derivative signal has the maximum slope and enables the laser spectrometer system to obtain optimal frequency stability. Under this optimal modulation, the third-derivative signal is fed into the laser PZT via a feedback control loop. Without a second identical laser system, we estimate the frequency stability from the error signal after locking by converting the error voltage to the frequency change. The frequency stability is estimated to be better than 10 kHz, corresponding to a relative value of 2.2×10^{-11}. The error signal is recorded by a chart recorder with a response time slightly lower than 1 s and is shown in Fig. 5.6. The SNR of 1000 at 1 s time constant and the linewidth of 7.5 MHz imply that the optimum stability is $1.6 \times 10^{-11}\tau^{-1/2}$ assuming a white frequency fluctuation. Therefore, the stability estimated from the error signal is quite reasonable. When an averaging time is 4000 s, the frequency stability is predicted to be 2.5×10^{-13} which is not far from the iodine-stabilized He-Ne lasers at 633 nm. Although the feedback loop is not optimized, our laser system obtains good frequency stability. For comparison, T. Masuda and coworkers [7] reported the frequency stabilization of a diode laser to the hyperfine component *f* of P(84) 5-5 transition and the stability they achieved is only 300 kHz.

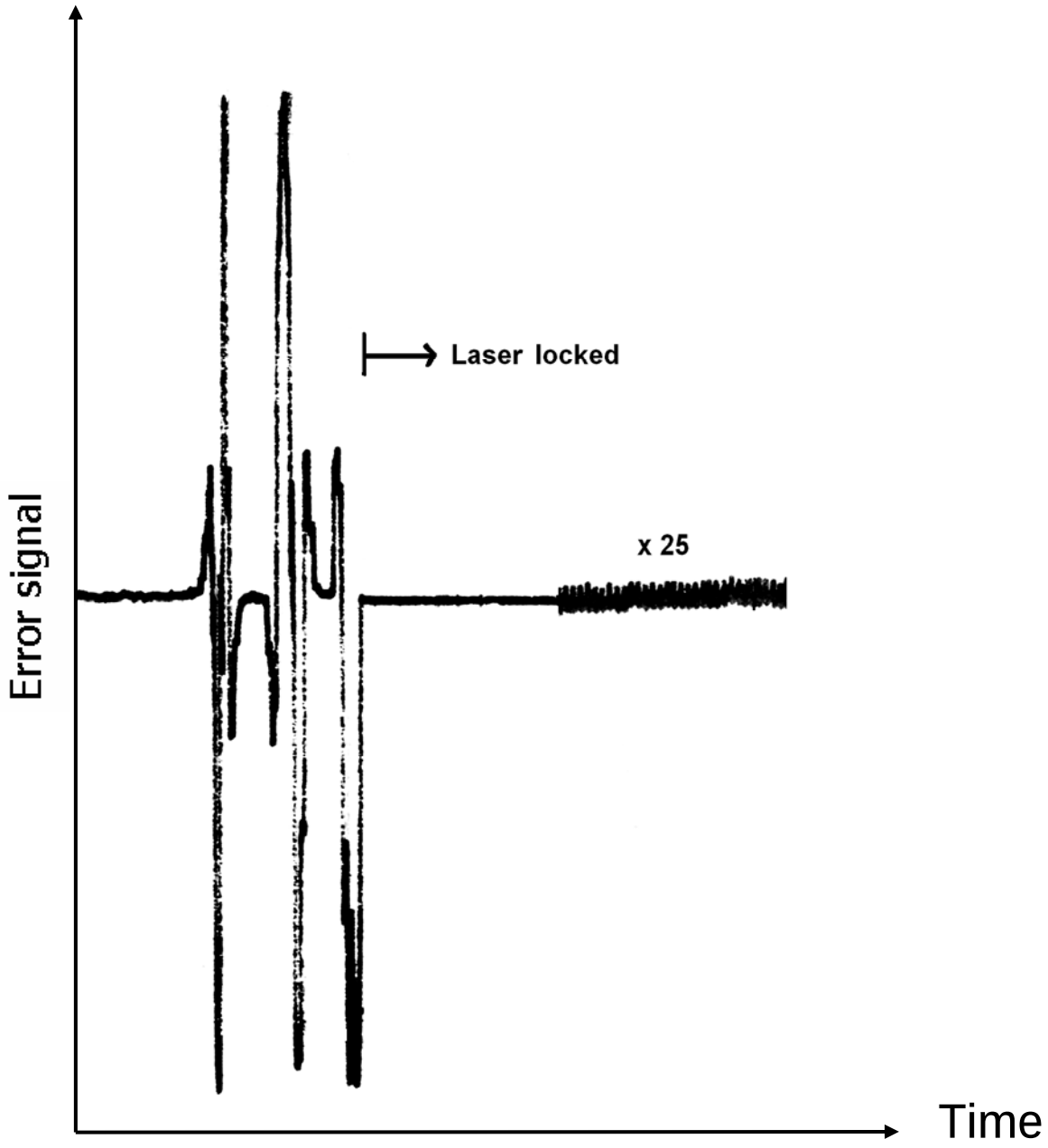

Fig. 5.6. Error signal of the hyperfine component *o* after locking is recorded by a chart recorder. The ECDL is frequency stabilized to it. The frequency stability is estimated to be better than 10 kHz, corresponding to a relative value of 2.2×10^{-11}.

5.4 Conclusions

We have developed a simple and compact diode laser stabilization system. Hyperfine structure components of P(84) 5-5 transition of molecular iodine ($^{127}I_2$) at 657.483 nm are observed with a SNR of 1000 at 1 s time constant. Our system is less complex than the systems in the previous literatures [7,10]. The diode laser is frequency stabilized to the hyperfine component *o* of the saturated absorption signal. The frequency stability better than 10 kHz is achieved. It is expected that the stability can be further improved by employing higher modulation frequency and by optimizing the feedback loop.

In our system we modulate the frequency by current modulation instead of cavity length modulation by PZT employed by others. Our results indicate that the amplitude modulation induced by current modulation is comparable to PZT modulation and the amplitude modulation induced drift is negligible. We demonstrate that the SNR and stability can be increased by the current modulation since we can modulate the laser at frequency higher than PZT modulation. Our scheme can be applied to ECDL at other wavelengths.

References

[1] H. R. Simonsen, IEEE Trans. Instrum. Meas. **46**, 141 (1997).

[2] C. S. Edwards, G. P. Barwood, P. Gill, and W. R. C. Rowley, Metrologia **36,** 41 (1999).

[3] J. Lazar, O. Cíp, and P. Jedlicka, Appl. Opt. **39**, 3085 (2000).

[4] M. Merimaa, P. Kokkonen, K. Nyholm, and E. Ikonen, Metrologia **38,** 311 (2001).

[5] C. S. Edwards, G. P. Barwood, P. Gill, and W. R. C. Rowley, Electron. Lett. **31**, 796 (1995).

[6] C. S. Edward, G. P. Barwood, P. Gill, F. Rodríguez-Llorente, and W. R. C. Rowley, Opt. Commun. **132,** 94 (1996).

[7] T. Masuda, T. Kimura, T. Tako, and A. Morinaga, Jpn. J. Appl. Phys. **36**, L1443 (1997).

[8] T. J. Quinn, Metrologia **40,** 103 (2003).

[9] M. S. Huang, M. H. Lu, and J. T. Shy, Rev. Sci. Instrum. **73,** 3747 (2002).

[10] T. Kurosu, J. Ishikawa, and N. Ito, Jpn. J. Appl. Phys. **36**, 4513 (1997).

[11] M. G. Littman, Opt. Lett. **3**, 138 (1978).

[12] M. Nakazawa, J. Appl. Phys. **59**, 2297 (1986).

Chapter 6 Summary and Future Works

6.1 Summary

We have verified that the Lorentzian linewidth can be easily determined by using the dependence of the peak amplitude of the third-derivative signal on the modulation width. This method should be used to determine the linewidth of hyperfine structure component of saturation absorption spectrum. Because the 532 nm system has proved to be one of the best practical optical frequency standards, we have used this method to investigate pressure broadening and power broadening of the a_{10} component of R(56) 32-0 transition of $^{127}I_2$ at 532 nm systematically. The pressure broadened linewidth is quite linear with vapor pressure. The slope of the linear fit is 63 kHz/Pa for FWHM width. From the power broadening parameter the saturation intensity is obtained to be 5.76 mW/mm^2. These characteristics can be as reference for those who study 532 nm systems for precision spectroscopy.

The hyperfine structure components of I_2 spectra have also shown to be suitable frequency references for laser frequency stabilization. Moreover, I_2 also provides a good subject with which to test theoretical models for Hamiltonian of hyperfine interactions. For these interactions, the measured hyperfine splittings are fitted to a four-term Hamiltonian and the corresponding hyperfine constants could be obtained. In general, the hyperfine splitting is measured by heterodyne technique. However, not every laboratory could set up two iodine-stabilized lasers for measuring hyperfine splitting.

For this reason, we study a method replacing heterodyne technique to measure the hyperfine splittings. We use the R(56) 32-0 transition of $^{127}I_2$ at 532 nm as an example to investigate this method in which uses only one laser with a double-passed acousto-optic modulator frequency shifter. Consequently, we have successfully measured the hyperfine splitting of R(56) 32-0 transition. Using the a_{10} component as a reference, the difference of the

hyperfine splitting between Consultative Committee for Length and our results is within 20 kHz.

Except for the diode-pumped, frequency doubled Nd:YAG laser at 532 nm, we are also interesting in using diode lasers for frequency stabilization because of their smaller size, larger tuning range, higher power, and compactness. Frequency stabilization of the external cavity diode laser (ECDL) to the iodine hyperfine structure components using extra-cavity iodine cell has been extensively studied and reported.

The general modulation scheme in which modulates the cavity length of the ECDL using a piezoelectric transducer limits the modulation frequency to <10 kHz. To reduce the noise, we choose to modulate the laser frequency by modulating the diode current instead of the cavity length by PZT.

To further investigate the high resolution spectroscopy of the Ca and to study an attractive alternative for red diode laser systems locked to iodine, we develop a stable diode laser system at 657 nm as a stable light source. We use the 657 nm ECDL to investigate the saturation spectrum of the hyperfine structure components of P(84) 5-5 transition of $^{127}I_2$ at 657.483 nm for frequency stabilization of our ECDL laser.

We have obtained the hyperfine structure components of P(84) 5-5 transition with a SNR of 1000 at 1 s time constant. The diode laser is frequency stabilized to the hyperfine component *o* of the saturated absorption signal. The frequency stability better than 10 kHz is achieved.

6.2 Future Works

In the experiment of the AOM frequency shifter, the differences of the hyperfine splitting between our results and CCL (1.5 kHz uncertainty) are below 20 kHz. The contributions to the discrepancy include the frequency counting error, different iodine cells, and different

experimental conditions for frequency locking and saturation spectroscopy. Those can be easily improved. For example, we can lock a voltage controlled oscillator to the measured hyperfine peak and measure the frequency more carefully. To reduce the error from pressure shift and impurities in different cells we plan to make a special cell in which two cells are connected by a tube.

In the future we will improve the accuracy of this method by using the above thoughts and use it to measure the hyperfine splittings of 16 iodine transitions we have observed at 531 nm using a frequency doubled alpha-distributed feedback diode laser.

In the experiment of using diode lasers at 657 nm for frequency stabilization, we will further improve the stability by employing higher modulation frequency and by optimizing the feedback loop. It will be a more stable light source to investigate the high resolution spectroscopy. Our scheme can be applied to ECDL at other wavelengths.

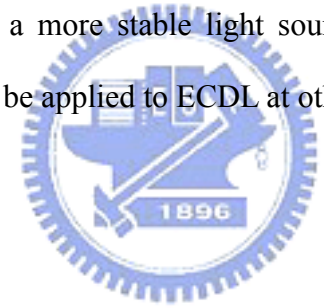

著 作 目 錄

期刊論文

[1] Hui-Mei Fang, Shing-Chung Wang, and Jow-Tsong Shy, “Frequency stabilization of an external cavity diode laser to molecular iodine at 657.483 nm,” to be published in Applied Optics.

[2] Hui-Mei Fang, S. C. Wang, and Jow-Tsong Shy, “Pressure and power broadening of the a_{10} component of R(56) 32-0 transition of molecular iodine at 532 nm,” to be published in Optics Communications.

[3] Hui-Mei Fang, S. C. Wang, Li-Ch’un Liu, Wang-Yau Cheng, Kao-Yu Wu, and Jow-Tsong Shy, “Measurement of Hyperfine Splitting of Molecular Iodine at 532 nm by Double-Passed Acousto-Optic Modulator Frequency Shifter,” submitted to Jpn. J. Appl. Phys.